

Noisy Analysis of Quantum SMOTE on Condition Monitoring and Fault Classification in Industrial and Energy Systems

Amit S. Patel^{1*}, Himanshukumar R. Patel^{2*} and Bikash K. Behera³

¹Department of Mechanical Engineering, Dharmsinh Desai University, College Road, Nadiad, 387001, Gujarat, India.

²Department of Instrumentation & Control Engineering, Dharmsinh Desai University, College Road, Nadiad, 387001, Gujarat, India.

³ Bikash's Quantum (OPC) Pvt. Ltd., Balindi, Mohanpur, 741246, West Bengal, India.

*Corresponding author(s). E-mail(s): aspatel.mh@ddu.ac.in;
himanshupatel.ic@ddu.ac.in;
Contributing authors: bikas.riki@gmail.com;

Abstract

Imbalanced datasets are a fundamental issue in industrial condition monitoring and fault classification pipelines, causing classical machine learning models to overfit the majority classes while failing to learn the minority fault patterns. This paper presents a detailed benchmarking and robustness investigation of classical classifiers under (i) class imbalance mitigation using the Quantum Synthetic Minority Oversampling Technique (QSMOTE) and (ii) quantum-inspired perturbations modelled using six noise channels. Four different datasets, the Solar Panel Image Dataset (SPID), the CWRU Bearing Dataset (CWRUBD), the Engine Failure Detection Dataset (EFDD), and the Industrial Fault Detection Dataset (IFDD), are tested across multi-class scenarios to determine the universality of these impacts. The results show that QSMOTE consistently corrects distributional skew and significantly enhances the performance of non-linear classifiers such as Random Forests (RF), Support Vector Machines (SVM), and Decision Trees (DT), yielding improvements of up to 170% on EFDD and achieving near-perfect accuracy (≥ 0.99) on IFDD. Linear and probabilistic models, such as Linear Regression (LR) and Naive Bayes (NB), produce mixed results, with significant degradation in overlapping feature spaces due to interpolation-induced

boundary distortion. A parallel robustness analysis under bit-flip, phase-flip, bit-phase-flip, depolarizing, amplitude damping, and phase damping noise reveals that ensemble models (RF) and margin-based learners (SVM) maintain strong resilience, often preserving over 95% of baseline accuracy even under maximum noise. In contrast, NB and DT show substantial instability, especially on high-variance datasets. The findings establish a rigorous baseline for understanding how classical models behave under realistic imbalance and quantum-inspired noise, while motivating the development of advanced quantum-inspired resampling and noise-resilient learning frameworks for next-generation industrial AI systems.

Keywords: Quantum Smote, imbalanced datasets, condition monitoring, solar panel surface defects, bearing fault detection, engine failure detection

1 Introduction

1.1 Context and Motivation

Modern industrial, manufacturing, and energy infrastructures are increasingly equipped with large-scale sensing, monitoring, and control systems that continuously generate multimodal data for predictive maintenance and fault diagnosis. As these systems evolve into highly automated and interconnected Industry 4.0 environments, the need for reliable, noise-resilient, and imbalance-aware classification models has become critical [1, 2]. Real-world machine-condition datasets such as Solar Panel Image Dataset (SPID), CWRU Bearing Dataset (CWRUBD), Engine Failure Detection Dataset (EFDD), and Industrial Fault Detection Dataset (IFDD) are well-known for exhibiting severe class imbalance, where fault conditions are significantly under-represented compared to normal operating states. This imbalance leads to biased decision boundaries, poor generalization, and unstable performance in both classical and advanced machine learning (ML) models [3, 4]. Edge-deployed systems, including rotating machinery, induction motors, wind turbines, and industrial pumps, often function in noisy environments with signal corruption caused by sensor degradation, electromagnetic interference, environmental disturbances, or hardware faults [5, 6]. These conditions encourage evaluating ML models not just in clean settings, but also under quantum-inspired noise models, which simulate worst-case perturbations relevant for developing quantum-sensing, quantum-communication, and post-quantum environments [7]. As a result, understanding how noise impacts classifier stability is critical when constructing robust diagnostic pipelines.

The Synthetic Minority Oversampling Technique (SMOTE) is a popular strategy for addressing class imbalance. It produces interpolated minority samples to counteract skewed class distributions [3]. SMOTE has demonstrated effectiveness in a variety of fields, including cybersecurity, healthcare, and industrial fault diagnosis. However, classical SMOTE does not take non-linear structure, feature-space restrictions, or noise robustness into account. These restrictions encourage the exploration of quantum-inspired balancing approaches that use the geometry of quantum states for more

expressive minority-sample synthesis [8–10]. Furthermore, the rise of quantum machine learning (QML) opens up new possibilities for creating high-fidelity synthetic samples, boosting minority-class representation, and increasing robustness to perturbations. Quantum Boltzmann Machines (QBM), quantum kernels, and quantum generative models have demonstrated promising results in learning complicated distributions [11, 12]. Integrating quantum-inspired techniques into traditional fault-diagnostic pipelines is a promising route for next-generation condition monitoring systems. In conclusion, the combination of class imbalance, quantum-like noise, and model robustness requirements creates an urgent need for current resampling and assessment frameworks. This motivates the current study, in which we conduct a thorough examination of quantum SMOTE and quantum-noise stability across numerous industrial datasets, ultimately laying the framework for quantum-inspired oversampling and robustness-aware fault-diagnostic systems.

1.2 Gap Analysis

Despite substantial breakthroughs in ML-based fault diagnosis and imbalance mitigation strategies, some major research gaps remain unaddressed in the context of industrial and energy-system condition monitoring. The majority of recent works on fault classification rely on clean or minimally noisy environments, assuming trustworthy sensor measurements and robust acquisition hardware [5, 13]. However, real-world industrial systems are frequently exposed to strong stochastic disturbances, including mechanical vibrations, temperature fluctuations, electromagnetic interference, and sensor degradation. These noise patterns resemble complex non-classical transformations, yet the robustness of classical models is rarely evaluated under structured, physics-informed noise models, such as quantum-inspired channels such as bit-flip (BF), depolarizing (DP), and amplitude damping (AD). This leaves a gap in understanding how modern classifiers respond to worst-case perturbations that may emerge in next-generation cyber-physical and quantum-enabled infrastructures. Second, although class imbalance is widely acknowledged as a central challenge in predictive maintenance, most studies rely on classical oversampling methods such as SMOTE or its variants [3, 14]. While these algorithms improve minority representation, they do not explicitly preserve the geometric structure or manifold constraints of high-dimensional industrial datasets. Prior research indicates that interpolated synthetic samples can unintentionally distort the boundary between overlapping classes, reducing linear-model performance and introducing over-generalization [4, 15]. More importantly, conventional resampling does not address robustness to noise, making the augmented datasets vulnerable when downstream classifiers operate under harsh environmental conditions.

Third, although QML has recently demonstrated powerful capabilities in distribution learning, expressive data encoding, and sampling [9, 10], its potential to improve imbalance mitigation and robustness in industrial classification remains largely unexplored. Quantum generative models, such as QBM and quantum generative adversarial network (QGANs), offer natural advantages for producing complex synthetic samples that respect underlying data geometry [11, 12]. However, no prior work has systematically benchmarked classical oversampling methods against quantum-noise

perturbations across multiple real-world fault-diagnosis datasets. Finally, although several studies investigate noise tolerance in quantum circuits and quantum classifiers [16, 17], there is no existing framework that jointly evaluates (i) imbalance-handling effectiveness and (ii) noise robustness across diverse classical algorithms. This gap is particularly critical for industrial deployments where both minority-class scarcity and environmental noise co-occur. In summary, the literature lacks a unified benchmarking and analytical framework that examines:

- 1) How classical SMOTE-enabled models perform under quantum-inspired noise,
- 2) Which model families (linear, probabilistic, margin-based, or ensemble-based) degrade least under structured perturbations, and
- 3) What opportunities exist for quantum-inspired resampling to enhance robustness across heterogeneous datasets.

The present work addresses these gaps through a comprehensive empirical study spanning four industrial datasets, five classical ML models, six quantum-noise channels, and Quantum SMOTE (QSMOTE)-based imbalance mitigation, providing the first systematic connection between imbalanced-learning analysis and quantum-noise robustness evaluation.

1.3 Novelty and Contributions

Although prior studies have explored class imbalance mitigation and ML robustness independently, no existing work provides a unified framework that jointly analyzes (i) the effectiveness of oversampling on multi-class industrial datasets and (ii) the resilience of classical models under structured, quantum-inspired noise perturbations. This manuscript fills this critical gap by introducing the first comprehensive evaluation pipeline that integrates QSMOTE-based balancing with quantum-noise stress testing across four industrial and energy-system fault diagnosis datasets. The novelty of this work lies in demonstrating how conventional resampling strategies behave when downstream classifiers operate under quantum-inspired noise channels an emerging challenge for future cyber-physical and quantum-enabled monitoring systems. Our framework systematically examines margin-based, ensemble-based, probabilistic, and tree-based models under harsh noise conditions, offering new insights into structural robustness, noise sensitivity, and dataset-dependent vulnerability patterns. Furthermore, by comparing performance before and after QSMOTE across six noise channels, this work demonstrates how imbalance correction interacts with noise resilience, showing strengths and limitations that have not been previously reported. Overall, this study is a first-of-its-kind benchmarking study that integrates imbalance handling, classical-model resilience, and quantum-noise perturbation analysis into a unified methodology, providing actionable insights for developing more stable, noise-tolerant, and balanced data-driven fault classification pipelines. The primary contributions of this research are summarized below:

- 1) We develop the first integrated evaluation setup combining QSMOTE-based imbalance correction with quantum-inspired noise injection, enabling joint assessment of classification stability and noise robustness across diverse industrial datasets.

- 2) We conduct experiments on four major fault-diagnosis datasets (SPID, CWRUBD, EFDD, and IFDD), covering multi-class setups, establishing consistent patterns of model sensitivity and resilience.
- 3) We evaluate classifiers under six quantum-inspired noise models: BF, phase-flip (PF), bit-phase-flip (BPF), DP, AD, and phase damping (PD), providing the first systematic robustness study of classical ML models under structured quantum perturbations.
- 4) We show how QSMOTE reshapes accuracy, precision, recall, and F1-score under noisy conditions, revealing which model families benefit most (random forest (RF), decision tree (DT), and support vector machine (SVM)) and which degrade under oversampling (logistic regression (LR) and naive bayes (NB)).
- 5) We derive a consistent, dataset-wide robustness hierarchy (e.g., RF > SVM > LR > NB/DT) across all noise channels, offering practitioners clear guidance for choosing resilient models.
- 6) We identify that EFDD and IFDD datasets exhibit substantially higher noise sensitivity, particularly for shallow probabilistic and tree-based models, highlighting the importance of dataset-specific robustness considerations.
- 7) Our findings motivate the development of quantum-inspired balancing frameworks (e.g., QSMOTE) that preserve feature-space geometry and enhance robustness beyond classical SMOTE.

Fig. 1 illustrates the complete experimental pipeline adopted in this work to evaluate the impact of QSMOTE and quantum-inspired noise models on classical ML-based fault classification in industrial and energy systems. The workflow begins with industrial datasets, which include sensor-based and image-based condition-monitoring data. Prior to learning, all datasets undergo preprocessing, such as feature normalization, encoding, and dimensionality reduction using principal component analysis (PCA) where applicable. This phase guarantees that feature representations are compact while retaining discriminative information, which is especially important for high-dimensional datasets like solar panel images and vibration signals. Next, QSMOTE analysis is used to address extreme class imbalances that are typical in real-world fault datasets. Unlike standard SMOTE, QSMOTE generates synthetic minority samples using quantum-inspired similarity estimates, resulting in a balanced class distribution while maintaining the feature space's geometric structure. The balancing method equalizes the minority and majority class populations, reducing prejudice throughout training. The balanced dataset is then fed into several classical ML models, such as LR, RF, SVM, DT, and NB. These models include linear, probabilistic, margin-based, and ensemble learners, allowing for a thorough comparison of algorithmic behaviour under balanced and noisy settings. To measure resilience, a quantum-inspired noisy analysis stage is used. Six noise channels (BF, PF, BPF, DP, AD, and PD) are injected to simulate structured disturbances similar to quantum decoherence and realistic sensor corruption. This stage assesses the stability of classical classifiers under gradually rising noise levels. Finally, the pipeline concludes with evaluation and results analysis, where model performance is quantified using accuracy, precision, recall, and F1-score. These metrics provide a holistic assessment of both classification effectiveness and robustness under imbalance correction and noise stress testing.

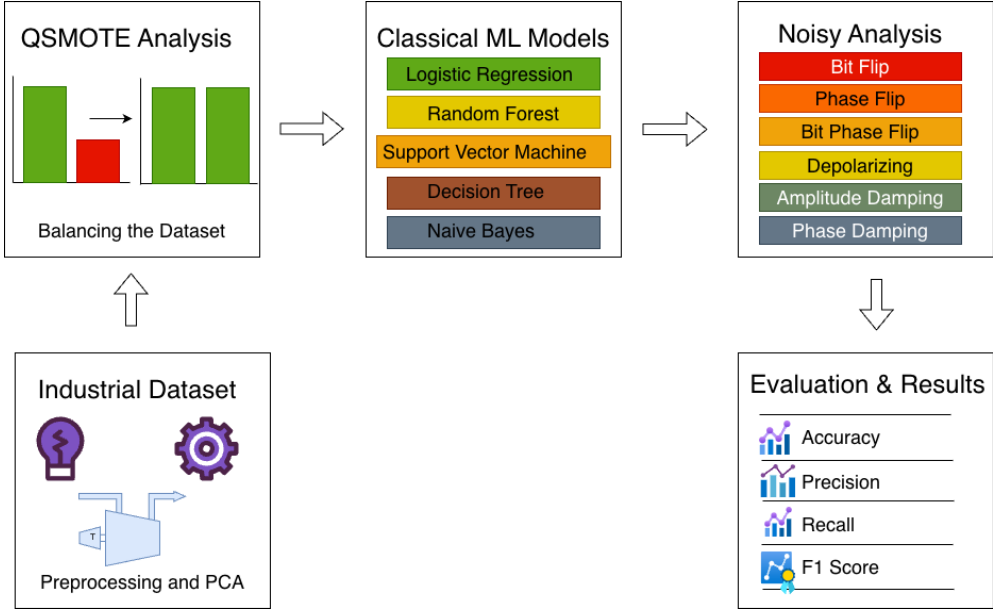


Fig. 1: Overall experimental workflow for QSMOTE-based imbalance mitigation and quantum-noise robustness analysis. Industrial datasets are first preprocessed and reduced using PCA, followed by class balancing through QSMOTE. The balanced data are evaluated using classical ML models (LR, RF, SVM, DT, and NB). Quantum-inspired noise channels including BF, PF, BPF, DP, AD, and PD are then injected to assess robustness. Model performance is finally quantified using accuracy, precision, recall, and F1-score.

1.4 Organization

The rest of the paper is organized as follows. Section 2 discusses the existing works related to class imbalance and ML models for fault diagnosis. Then, in Section 3, a detailed explanation of the proposed methodology is provided. Next, Section 4 provides the details on the dataset, preprocessing steps, hyperparameters, evaluation metrics and experimental results with a discussion. Finally, in Section 5, the conclusion is made with the future direction of research.

2 Related Works

Research on class imbalance handling, industrial fault diagnosis, and noise-robust ML has evolved significantly over the past decade. This section reviews the most relevant literature across three major themes: (i) imbalance mitigation and resampling techniques, (ii) classical ML models for condition monitoring, and (iii) robustness under noise and quantum-inspired corruption models.

2.1 Imbalance Mitigation and SMOTE-Based Resampling

Class imbalance is a well-documented challenge in industrial condition-monitoring datasets, where failure samples are rare compared to normal operation. Traditional oversampling and undersampling methods such as random oversampling, Tomek links, or cluster-based undersampling often struggle to preserve minority-class structure [3, 4]. The introduction of the SMOTE marked a pivotal advancement by generating synthetic minority samples through linear interpolation between feature-space neighbors [3]. Variants such as Borderline-SMOTE [18], Adaptive Synthetic Sampling (ADASYN) [19], and SMOTE-Tomek Links [20] further refine interpolation quality or perform noise-aware resampling. In fault diagnosis, SMOTE is frequently used to correct imbalance in vibration, acoustic, and multi-sensor health-monitoring datasets [21, 22]. Existing research, however, focuses mostly on performance improvements after balancing, rather than investigating how oversampled datasets behave under noise-corrupted assessment or in multi-class industrial contexts. This study contributes to the field by examining SMOTE’s impact not only on classification metrics but also on robustness against structured quantum-inspired noise.

2.2 Classical Machine Learning Models for Fault Diagnosis

Numerous classical models have been successfully deployed for industrial fault classification. Linear classifiers such as LR provide interpretable decision boundaries but often struggle with nonlinear relations common in mechanical and electrical systems [23]. Probabilistic models like NB are computationally efficient yet sensitive to feature correlation [24]. SVMs remain widely used in fault diagnosis due to their strong margin maximization properties and robustness to high-dimensional data [25]. Ensemble methods, including RF, have proven particularly effective for multi-class industrial datasets due to their ability to model complex nonlinear patterns [26]. While these models show strong baseline performance, prior work primarily evaluates them under noise-free conditions or simple stochastic corruptions (e.g., Gaussian noise). This paper extends prior studies by benchmarking models across six quantum-inspired noise channels, enabling a more realistic assessment of robustness for next-generation cyber-physical and quantum-touched diagnostic systems.

2.3 Noise Robustness and Quantum-Inspired Perturbation Models

ML robustness under various perturbation models has been explored in adversarial learning [27], random corruption studies [28], and sensor-noise simulations for industrial monitoring [29]. However, quantum-inspired noise originating from fundamental quantum channels such as BF, PF, DP, and AD/PD has recently gained interest due to the growing integration of quantum sensing and quantum communication in industrial IoT systems [30]. Prior works primarily analyze these channels in QML settings, studying their effect on quantum kernels, variational circuits, or entangled state discrimination [31, 32]. Yet, no existing work systematically evaluates how classical ML models behave when tested under quantum-inspired noise on multi-class industrial

datasets. This manuscript provides the first cross-dataset, cross-noise robustness analysis of LR, RF, SVM, NB, and DT under six quantum channels, bridging the gap between classical robustness research and quantum-influenced data degradation.

2.4 Positioning and Novelty of This Study

To the best of our knowledge, no prior study simultaneously examines: multi-class industrial datasets (SPID, CWRUBD, EFDD, IFDD), QSMOTE-based balancing effects, five classical classifier families, and quantum-inspired noise robustness across six channels. Existing literature treats these areas separately, whereas this work integrates them into a single, comprehensive robustness-oriented evaluation framework. This unified analysis is crucial as real-world industrial systems increasingly incorporate quantum communication links, quantum sensors, and hybrid classical-quantum environments.

3 Methodology

3.1 Problem Formulation and Overall Framework

In imbalanced classification problems, the training dataset $X = \{x_i \in \mathbb{R}^d\}_{i=1}^n$ with labels $y_i \in \mathcal{Y} = \{1, 2, \dots, K\}$ contains classes with highly unequal sample sizes. Let $N_\ell = |\{i : y_i = \ell\}|$ denote the number of samples in class ℓ , and define

$$N_{\max} = \max_{\ell \in \mathcal{Y}} N_\ell, \quad N_{\min} = \min_{\ell \in \mathcal{Y}} N_\ell, \quad (1)$$

where typically $N_{\min} \ll N_{\max}$. The objective is to construct an augmented dataset $(X_{\text{out}}, y_{\text{out}})$ that restores approximate balance across all classes while preserving the intrinsic manifold structure of the feature space. The proposed *QSMOTE* utilizes a three-stage hybrid pipeline that blends classical clustering and quantum-inspired geometric reasoning:

1. Cluster Formation: The K -means algorithm partitions the feature matrix X into K clusters, resulting in centroids $\{\mu_j\}_{j=1}^K$. Each sample x is assigned to its nearest centroid $c(x)$, which offers a local geometric framework for creating synthetic samples.
2. Quantum similarity estimation: The normalized feature representations of each minority instance x and centroid $c(x)$ are treated as amplitude-encoded quantum states. The *compact swap test* is used to calculate the quantum overlap or inner product $\langle M | C \rangle$ of these states. The *quantum-inspired angle* $\alpha(x, c)$ quantifies the alignment between x and $c(x)$ in a normalized feature space.
3. Synthetic Sample Generation: The angle $\alpha(x, c)$ determines the step size and direction for creating a new synthetic instance \tilde{x} along the vector connecting x and $c(x)$. Larger angular deviations result in correspondingly larger synthetic displacements, allowing adaptive interpolation based on local cluster geometry. Repeating this method for all minority points results in an oversampled dataset that is consistent with the majority class distribution while minimizing redundancy.

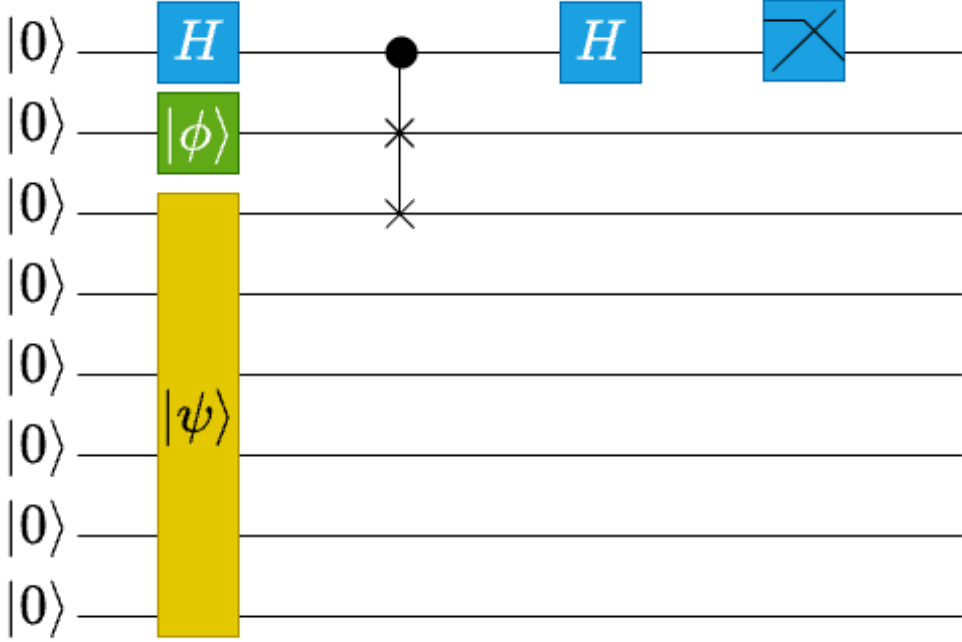


Fig. 2: Quantum circuit illustrating the compact swap test.

In essence, the QSMOTE framework integrates classical data topology (via clustering) with quantum-inspired similarity measurement (via the compact swap test). This integration introduces an angle-based mechanism for generating synthetic data that is both geometrically meaningful and statistically balanced. Unlike conventional SMOTE variants that rely solely on Euclidean interpolation, the proposed method leverages quantum overlap information to adaptively regulate the synthetic sampling process, ensuring improved diversity, cluster consistency, and minority-class representation in the resulting balanced dataset.

3.2 Compact Swap Test

The compact swap test is performed using two data points, centroid (C) and minority (M). Their quantum states can be written as,

$$\begin{aligned} |C\rangle &= \frac{1}{|C|} \sum_i c_i |i\rangle, \\ |M\rangle &= \frac{1}{|M|} \sum_i m_i |i\rangle, \end{aligned} \tag{2}$$

where, $|C|$ and $|M|$ are the normalization constants, and c_i and m_i are the feature values for data points C and M respectively. The inner product between $|C\rangle$ and $|M\rangle$ is calculated using the compact swap test circuit shown in Fig. 2. This is a resource-efficient method to estimate the overlap between two quantum states $|C\rangle$ and $|M\rangle$. First, the quantum states $|\psi\rangle$ and $|\phi\rangle$ are defined as follows:

$$\begin{aligned} |\psi\rangle &= \frac{|0\rangle \otimes |C\rangle + |1\rangle \otimes |M\rangle}{\sqrt{2}}, \\ |\phi\rangle &= \frac{|C| |0\rangle - |M| |1\rangle}{\sqrt{Z}} = \frac{C |0\rangle - M |1\rangle}{\sqrt{Z}}, \\ Z &= |C|^2 + |M|^2. \end{aligned} \quad (3)$$

The top qubit, initialized in $|0\rangle$, is put into superposition using a Hadamard gate and acts as a control for the subsequent operations involving the states $|\phi\rangle$ (green box) and $|\psi\rangle$ (yellow box). Through controlled operations, the ancilla qubit effectively compares the two states, and a second Hadamard followed by measurement encodes the overlap information into the ancilla's outcome. The initial state of the quantum circuit is given as,

$$\begin{aligned} &|+\rangle |\phi\rangle |\psi\rangle \\ &= \frac{1}{\sqrt{2}} (|0\rangle |\phi\rangle |\psi\rangle + |1\rangle |\phi\rangle |\psi\rangle) \\ &= \frac{1}{\sqrt{2}} (|0\rangle \left(\frac{|C| |0\rangle - |M| |1\rangle}{\sqrt{Z}} \right) \left(\frac{|0\rangle \otimes |C\rangle + |1\rangle \otimes |M\rangle}{\sqrt{2}} \right) \\ &\quad + |1\rangle \left(\frac{|C| |0\rangle - |M| |1\rangle}{\sqrt{Z}} \right) \left(\frac{|0\rangle \otimes |C\rangle + |1\rangle \otimes |M\rangle}{\sqrt{2}} \right)) \end{aligned} \quad (4)$$

After CSWAP operation, the expression becomes,

$$\begin{aligned} &\xrightarrow{\text{CSWAP}} \frac{1}{2\sqrt{Z}} ((C |0\rangle |0\rangle |0\rangle |C\rangle + C |0\rangle |0\rangle |1\rangle |M\rangle \\ &\quad - M |0\rangle |1\rangle |0\rangle |C\rangle - M |0\rangle |1\rangle |1\rangle |M\rangle) \\ &\quad + (C |1\rangle |0\rangle |0\rangle |C\rangle + C |1\rangle |1\rangle |0\rangle |M\rangle \\ &\quad - M |1\rangle |0\rangle |1\rangle |C\rangle - M |1\rangle |1\rangle |1\rangle |M\rangle)) \end{aligned} \quad (5)$$

After Hadamard application, the expression can be written as,

$$\begin{aligned} &\xrightarrow{H_1} \frac{1}{2\sqrt{Z}} ((C |+\rangle |0\rangle |0\rangle |C\rangle + C |+\rangle |0\rangle |1\rangle |M\rangle \\ &\quad - M |+\rangle |1\rangle |0\rangle |C\rangle - M |+\rangle |1\rangle |1\rangle |M\rangle)) \end{aligned}$$

$$\begin{aligned}
& + (C |-\rangle |0\rangle |0\rangle |C\rangle + C |-\rangle |1\rangle |0\rangle |M\rangle \\
& - M |-\rangle |0\rangle |1\rangle |C\rangle - M |-\rangle |1\rangle |1\rangle |M\rangle)
\end{aligned} \tag{6}$$

The probability of measuring the ancilla qubit in the ‘0’ state is calculated as,

$$\begin{aligned}
P_0 = \frac{1}{8Z} & \left| C |0\rangle |0\rangle |C\rangle + C |0\rangle |1\rangle |M\rangle \right. \\
& - M |1\rangle |0\rangle |C\rangle - M |1\rangle |1\rangle |M\rangle \\
& + C |0\rangle |0\rangle |C\rangle + C |1\rangle |0\rangle |M\rangle \\
& \left. - M |0\rangle |1\rangle |C\rangle - M |1\rangle |1\rangle |M\rangle \right|^2
\end{aligned} \tag{7}$$

After simplifying the above expression, finally, the inner product between the centroid and minority data point is found to be,

$$\langle M | C \rangle = \frac{(3 - 4P_0)Z}{2|C|.|M|} \tag{8}$$

Alternatively, the probability of obtaining $|0\rangle$ on the ancilla is

$$P(0) = \frac{1}{4} \left(3 - \frac{2|C|.|M| \langle M | C \rangle}{Z} \right), \tag{9}$$

from which the overlap $\langle M | C \rangle$ can be extracted. This compact variant of the SWAP test is particularly useful in NISQ-era devices, as it reduces the number of qubits required while still enabling reliable comparison of quantum states for applications in verification, quantum communication, and ML. The compact swap test method shown in algorithm 1 computes a quantum-inspired angle between two vectors c and m by encoding their normalized forms into a quantum circuit. It first prepares an ancilla qubit in a superposition state using a Hadamard gate, then encodes a rotation based on the relative norms of the vectors. The vectors themselves are concatenated, normalized, and initialized on the remaining qubits. A controlled-SWAP operation followed by another Hadamard on the ancilla allows interference that encodes the inner product between c and m . Measuring the ancilla and calculating the probability of outcome ‘0’ enables estimation of the inner product, which is clipped to the valid range and converted to an angle using the arccos function. This angle reflects the similarity or quantum-inspired distance between the two input vectors.

3.3 Quantum SMOTE

Let $X = \{x_i \in \mathbb{R}^d\}_{i=1}^n$ be the feature set with labels $y_i \in \mathcal{Y}$ and let $\mathcal{L}_{\min} \subset \mathcal{Y}$ denote the set of minority labels. We assume features are standardized (zero mean, unit variance per coordinate) and write

$$N_\ell := |\{i : y_i = \ell\}|, \quad M := \max_{\ell \in \mathcal{Y}} N_\ell.$$

Algorithm 1 Compact Swap Test

Input: Vectors c, m
Output: Quantum-inspired angle between c and m

- 1: Convert c and m to numpy arrays of type float64
- 2: Compute norms: $norm_c \leftarrow \|c\|$, $norm_m \leftarrow \|m\|$
- 3: Compute normalization factor: $Z \leftarrow norm_c^2 + norm_m^2$
- 4: Set number of qubits $n \leftarrow \log_2(\text{len}(c)) + 3$
- 5: Initialize quantum circuit qc with n qubits and 1 classical bit
- 6: Apply Hadamard gate on qubit 0 (ancilla)
- 7: Compute angle $\theta \leftarrow 2 \cdot \arctan(norm_m/norm_c)$
- 8: Apply single-qubit rotation $u(\theta, \pi, 0)$ on qubit 1
- 9: Normalize vectors: $c \leftarrow c/norm_c$, $m \leftarrow m/norm_m$
- 10: Concatenate to form $\psi \leftarrow [c, m]$
- 11: Normalize $\psi \leftarrow \psi/\|\psi\|$
- 12: Initialize ψ on qubits 2 to $n - 1$ of qc
- 13: Apply controlled-SWAP gate with control qubit 0 and target qubits 1 and 2
- 14: Apply Hadamard gate on qubit 0
- 15: Measure qubit 0
- 16: Run qc on AerSimulator with 1000 shots
- 17: Get counts for outcome '0': c_0
- 18: Compute probability $p_0 \leftarrow c_0/1000$
- 19: Compute inner product $inner_product \leftarrow (3 - 4p_0) \cdot Z/(2 \cdot norm_c \cdot norm_m)$
- 20: Clip value: $final \leftarrow \text{clip}(inner_product, -1.0, 1.0)$
- 21: Compute angle $\phi \leftarrow \arccos(final)$
- 22: **return** ϕ

A K -means model fitted on X yields centroids $\{\mu_j\}_{j=1}^K$. Each point x is associated to its nearest centroid

$$\text{cid}(x) := \arg \min_{1 \leq j \leq K} \|x - \mu_j\|_2, \quad c(x) := \mu_{\text{cid}(x)}. \quad (10)$$

For each $\ell \in \mathcal{L}_{\min}$, the number of synthetic samples to be generated is

$$\text{need}_\ell = M - N_\ell, \quad \text{if } \text{need}_\ell > 0. \quad (11)$$

Given a nonzero vector $v \in \mathbb{R}^d$, define its amplitude-encoded quantum state

$$|\psi_v\rangle := \frac{1}{\|v\|_2} \sum_{m=1}^d v_m |m\rangle, \quad v \neq 0. \quad (12)$$

For a minority sample x and its assigned centroid $c = c(x)$, the (squared) state overlap is

$$s(x, c) := \langle \psi_x | \psi_c \rangle = \langle M | C \rangle = \cos \alpha(x, c), \quad (13)$$

where $\alpha(x, c)$ is the geometric angle between x and c . A compact swap test provides an unbiased estimator of $s(x, c)$ via the ancilla-0 probability p_0 given in Eq. (9). We define the *quantum-inspired angle*

$$\alpha(x, c) := \cos^{-1}(s(x, c)), \quad (14)$$

For x , define the unit direction pointing from x to its centroid:

$$\hat{d}(x, c) := \frac{c - x}{\|c - x\|_2}. \quad (15)$$

Let $\kappa > 0$ be the user-chosen split factor (denoted `split_factor` in Algorithm 2). For each synthetic draw, sample a scalar step length

$$r \sim \text{Unif}\left(0, \frac{\alpha(x, c)}{\kappa}\right). \quad (16)$$

This linear map couples the step scale to the quantum angle: when x is already well aligned with c (α small), r concentrates near 0; when x is poorly aligned (α large), r admits larger values, encouraging stronger movement toward the cluster structure. A single synthetic sample associated with a minority point x and centroid $c = c(x)$ is constructed as

$$\tilde{x} = x + r \hat{d}(x, c). \quad (17)$$

The synthetic set for class ℓ is generated by repeating Eq. (17) independently need_ℓ times for randomly chosen minority seeds x with $y = \ell$. Stacking all generated \tilde{x} across $\ell \in \mathcal{L}_{\min}$ produces the oversampled matrix X_{out} and corresponding labels y_{out} . The method has the following consequences:

1. **Adaptivity to cluster geometry:** The step direction is *cluster-informed* via $c = c(x)$, and the step length adapts to the *quantum similarity* between x and c through $\alpha(x, c)$ in Eq. (14).
2. **Scale compatibility:** Because r is dimensionless while Eq. (17) outputs in feature units, standardization of X is assumed so that angular scales translate meaningfully into step magnitudes.
3. **Convex movement:** If one wishes to constrain synthetic samples strictly within the ray segment from x towards c , the optional projection

$$\tilde{x} \leftarrow x + \min\{r, \|c - x\|_2\} \hat{d}(x, c)$$

can be applied; Algorithm 2 uses Eq. (17) without this clamp.

Algorithm 2 Quantum SMOTE

Input: Feature matrix X , label vector y , minority labels $minority_labels$, number of clusters $clusters$, split factor $split_factor$

Output: Oversampled feature matrix X_out , label vector y_out

```
1: Import KMeans and numpy
2: Initialize  $X\_out \leftarrow X$ ,  $y\_out \leftarrow y$ 
3: Fit KMeans with  $clusters$  on  $X$  to get centroids
4: for each label  $lbl$  in  $minority\_labels$  do
5:     Extract minority samples  $minority\_class \leftarrow X[y == lbl]$ 
6: end for
7: Compute majority class count  $majority\_count \leftarrow \max(\text{counts of each class})$ 
8: for each minority class array do
9:     Compute number of new samples needed  $need \leftarrow majority\_count - \text{len}(\text{minority class})$ 
10:    end for
11:    for each minority label  $lbl$  and corresponding  $need$  do
12:        if  $need = 0$  or minority class is empty then continue
13:        end if
14:        Initialize empty list  $synth\_list$ 
15:        for  $i = 1$  to  $need$  do
16:            Pick random sample  $x$  from minority class
17:            Predict cluster  $cluster\_id$  of  $x$  using KMeans
18:            Get cluster centroid  $centroid \leftarrow centroids[cluster\_id]$ 
19:            Compute quantum-inspired angle  $angle \leftarrow compact\_swap\_test(x, centroid)$ 
20:            Sample step fraction  $frac \sim \text{Uniform}(0, angle/split\_factor)$ 
21:            Compute direction  $direction \leftarrow centroid - x$ 
22:            if  $\text{norm}(direction) > 0$  then
23:                Normalize  $direction \leftarrow direction / \|direction\|$ 
24:            else
25:                Assign tiny random normalized direction
26:            end if
27:            Generate synthetic sample  $synthetic \leftarrow x + direction * frac$ 
28:            Append  $synthetic$  to  $synth\_list$ 
29:        end for
30:        if  $synth\_list$  is not empty then
31:            Stack  $synth\_list$  to array
32:            Append synthetic samples to  $X\_out$ , append labels to  $y\_out$ 
33:        end if
34:    end for
35: return  $X\_out, y\_out$ 
```

The QSMOTE method shown in Algorithm 2 generates synthetic samples for minority classes in an imbalanced dataset using a quantum-inspired approach. It first fits a KMeans clustering model on the feature matrix X to obtain cluster centroids.

For each minority class, it calculates the number of new samples required to match the majority class size. For each required synthetic sample, it randomly selects a minority instance and predicts its cluster to obtain the corresponding centroid. It then computes a quantum-inspired angle between the sample and the centroid using the compact swap test method. A step fraction is sampled uniformly based on this angle and a split factor, and a direction vector from the sample to the centroid is computed and normalized. The synthetic sample is generated by moving along this direction scaled by the step fraction. All generated synthetic samples are concatenated to the original feature matrix and their labels to the label vector, producing a balanced dataset X_{out} and y_{out} for subsequent training of classical ML models.

4 Experimental Results

4.1 Datasets

The SPID comprises six distinct classes: bird-drop (162 images), clean (159 images), dusty (147 images), snow-covered (103 images), electrical-damage (87 images), and physical-damage (50 images) [33]. Each class represents a specific condition that can affect the efficiency and energy output of solar panels. While it offers diverse visual samples across categories, there is a noticeable imbalance in class distribution, with some categories (e.g., physical-damage) having fewer images compared to others (e.g., bird-drop). Then, the *CWRUBD* hosted on Kaggle [34] is used, which repackages the Case Western Reserve University (CWRU) Bearing Data Center's motor condition monitoring signals for ML research in industrial settings. For supervised learning, nine time-domain features are computed per segment; maximum, minimum, mean, standard deviation, RMS, skewness, kurtosis, crest factor, and form factor-over fixed windows of 2300 samples (i.e., 0.04s at 48 kHz). This segmentation yields labeled examples spanning multiple fault sizes, fault locations, and sensor positions, enabling robust classification and fault-identification studies on rotating machinery. The EFDD [35] is a synthetic collection simulating multi-sensor telemetry from automotive engines to support fault detection and severity classification. Records are time-stamped at 5-minute intervals beginning on December 24, 2024 at 10:00, and each row summarizes engine state via thermal, kinematic, vibration, and powertrain variables together with operational context and a discrete fault label. The dataset contains 1,000 samples and four target classes ($\text{Fault_Condition} \in \{0, 1, 2, 3\}$) ranging from normal to severe failure. The IFDD [36] is designed for automatic fault detection in Industry 4.0 applications that use IoT-based smart sensors. It collects industrial data from several sensors, such as temperature ($^{\circ}\text{C}$), vibration (m/s^2), pressure (kPa), flow rate (L/min), current (A), and voltage (V). Each instance represents a snapshot of equipment operating conditions and sensor information, enabling real-time monitoring and intelligent diagnostics. The dataset includes a `Fault_Type` variable that categorizes the system condition into four categories: 0 (Normal Operation), 1 (Overheating Fault), 2 (Leakage Fault), and 3 (Power Fluctuation Fault). 1000 samples are taken for the testing.

4.2 Preprocessing

In the preprocessing stage of SPID, first, the solar panel image dataset is downloaded from Kaggle and organized it into training and validation sets using TensorFlow’s `image_dataset_from_directory`, with an 80-20 split. Each image is resized to a fixed dimension of 244×244 pixels, batched, shuffled, and labeled according to its class. To visualize the data distribution, a few sample images are plotted along with their class names. For feature extraction, a ResNet50 model is pretrained on ImageNet, with the top classification layer removed and global average pooling applied, so that each image is mapped to a 2048-dimensional feature vector. These high-dimensional embeddings are then reduced to 32 principal components using PCA, ensuring compact yet informative features for downstream tasks. Finally, the reduced features and labels are stored in tabular form as Pandas DataFrames and exported as CSV files, making them suitable for classical ML pipelines for further experimentation. The CWRUBD is obtained from Kaggle, and the downloaded artifacts are counted to identify tabular files. The first available `.csv/.txt` file is ingested using `pandas.read_csv` with `sep=None` and the Python engine, allowing for automated delimiter inference. To standardize supervision targets, the original fault indicator column was renamed from `fault` to `label`. The `label` column is transformed to a string, and a deterministic integer encoding is created by enumerating unique class names in order of appearance (`label_map = {name: i}`). These identities are mapped back into the dataframe, so that `df["label"]` contains contiguous class IDs beginning with zero. For transparency and validation, the table’s head, mapping dictionary, unique ID set, and number of separate errors are displayed. This technique creates a clean, model-ready dataframe with a canonical `label` field (integers) while keeping a traceable mapping to the original categorical labels, which serves as the foundation for subsequent dataset segmentation and training procedures. In case of EFDD, all available CSV files are automatically detected and loaded into a `pandas.DataFrame`, where the target column is renamed to `label` for consistency and moved to the final position. The `Time_Stamp` attribute, when present, is converted into a datetime format for potential temporal analysis but excluded from training to avoid leakage. The categorical feature `Operational_Mode` is numerically encoded through a stable mapping $\text{Operational_Mode} \rightarrow 0, 1, 2, \dots, K - 1$ based on category appearance, with missing values replaced by a default “Unknown” class. Non-essential columns, including `Time_Stamp`, are dropped, and all numerical columns are memory-optimized by downcasting to lower-precision datatypes without compromising accuracy. The resulting dataset thus comprised normalized numerical and encoded categorical features, with the final structure denoted as $X \in \mathbb{R}^d$ and $y \in \{0, 1, 2, 3\}$, representing four distinct operational fault categories; No Fault, Overheating, Leakage, and Power Fluctuation, ready for further processing. The IFDD is retrieved using the `kagglehub` API, after which all available CSV or text files are programmatically identified and loaded into a unified `pandas.DataFrame`. The preprocessing pipeline standardized column names and structure by renaming the ground-truth column `Fault_Type` to `label` for consistency across experiments and positioning it as the final column. When present, the `Time_Stamp` attribute is parsed into a `datetime` format (errors coerced) to preserve temporal context but is excluded

from the feature set to prevent time-based leakage. All numeric sensor readings, including temperature, vibration, pressure, flow rate, current, and voltage, are retained as predictors, while non-informative attributes are dropped. Categorical features are normalized to string type, missing entries are replaced with the placeholder “Unknown” and a stable ordinal encoding map is applied based on the order of appearance to ensure deterministic label indices. Finally, numerical columns are downcast to `float32` or `int32` types using `pandas.to_numeric()` to reduce memory usage without loss of precision. The resulting dataset, organized as $X \in \mathbb{R}^d$ and $y \in \{0, 1, 2, 3\}$ representing No Fault, Overheating, Leakage, and Power Fluctuation classes, served as the clean and standardized input for the models.

4.3 Comparative Models

For comparison, several widely used classical ML models are evaluated that serve as strong baselines for classification tasks. LR is included as a simple yet effective linear model to test the separability of extracted features, while RF, an ensemble of DT, is employed to handle non-linear relationships and reduce overfitting. The SVM is chosen for its high-dimensional strength and ability to maximize class separation using optimal hyperplanes. NB, a lightweight probabilistic classifier based on Bayes’ theorem, is chosen for its efficiency and simplicity, despite the requirement of feature independence. Finally, the DT model is included because of its interpretability and ability to represent nonlinear decision limits with low complexity, making these models appropriate benchmarks against which to test our technique.

4.4 Hyperparameters and Metrics

Each baseline is trained with sensible, reproducible defaults and evaluated them using a consistent protocol. LR is run with `max_iter=500` on scaled features to ensure convergence under L2-regularized optimization. SVM uses an `rbf` kernel with `probability=True` (for downstream scoring/ROC needs) and is likewise fit on scaled inputs. GaussianNB is applied to scaled features without additional tuning, reflecting its parametric simplicity. Tree-based models operates on the unscaled tabular features: RF with `n_estimators=200`, `random_state=42`, and `n_jobs=-1` for robust, parallelized ensembling; and a DT with `random_state=42` as an interpretable non-linear baseline. For all models, stratified 5-fold cross-validation is performed on the training set to preserve class proportions and report mean \pm standard deviation of accuracy, precision, recall, and F1-score; the latter three are computed as weighted averages (with `zero_division=0`) to account for class imbalance. After cross-validation, each model is fit on the full training set and optionally assessed on a held-out test set to estimate generalization. Random seeds are fixed (`random_state=42`) for reproducibility.

4.5 Noise Model

The robustness of the proposed quantum algorithms is analyzed under six commonly used realistic noise models [37]. These include three unitary error models, bit flip, phase flip, and bit phase flip originating from imperfections in gate operations or interactions with the environment. In addition, the DP noise model captures random

Pauli errors occurring with equal probability, while PD and AD represent non-unitary processes that model decoherence and energy relaxation, respectively. Together, these models provide a comprehensive framework for assessing algorithmic stability under both discrete and continuous noise channels.

1) Bit Flip Noise: The bit flip channel represents the inversion of a qubit state $|0\rangle \leftrightarrow |1\rangle$ with probability η_B . Its Kraus operators are

$$E_0 = \sqrt{1 - \eta_B} I, \quad E_1 = \sqrt{\eta_B} X. \quad (18)$$

The resulting density matrix after noise application is

$$\zeta = (1 - \eta_B)\rho + \eta_B X \rho X. \quad (19)$$

2) Phase Flip Noise: This model introduces a phase error, flipping $|+\rangle$ to $|-\rangle$ with probability η_P . The Kraus operators are

$$E_0 = \sqrt{1 - \eta_P} I, \quad E_1 = \sqrt{\eta_P} Z, \quad (20)$$

and the noisy state evolves as

$$\zeta = (1 - \eta_P)\rho + \eta_P Z \rho Z. \quad (21)$$

3) Bit Phase Flip Noise: The bit phase flip model combines both bit and phase inversions, represented by the Pauli- Y operator, occurring with probability η_{BP} . The corresponding Kraus operators are

$$E_0 = \sqrt{1 - \eta_{BP}} I, \quad E_1 = \sqrt{\eta_{BP}} Y. \quad (22)$$

The transformed state is

$$\zeta = (1 - \eta_{BP})\rho + \eta_{BP} Y \rho Y. \quad (23)$$

4) Depolarizing Noise: DP noise randomizes the state by applying any Pauli error (X , Y , or Z) with equal probability $\eta_D/3$. The Kraus operators are

$$\begin{aligned} E_0 &= \sqrt{1 - \eta_D} I, & E_1 &= \sqrt{\eta_D/3} X, \\ E_2 &= \sqrt{\eta_D/3} Y, & E_3 &= \sqrt{\eta_D/3} Z. \end{aligned} \quad (24)$$

The effect on ρ is

$$\zeta = (1 - \eta_D)\rho + \frac{\eta_D}{3} (X \rho X + Y \rho Y + Z \rho Z). \quad (25)$$

5) Amplitude Damping Noise: AD models energy loss, such as spontaneous emission, where β_A is the probability of relaxation. Its Kraus operators are

$$E_0 = |0\rangle \langle 0| + \sqrt{1 - \beta_A} |1\rangle \langle 1|, \quad E_1 = \sqrt{\beta_A} |0\rangle \langle 1|, \quad (26)$$

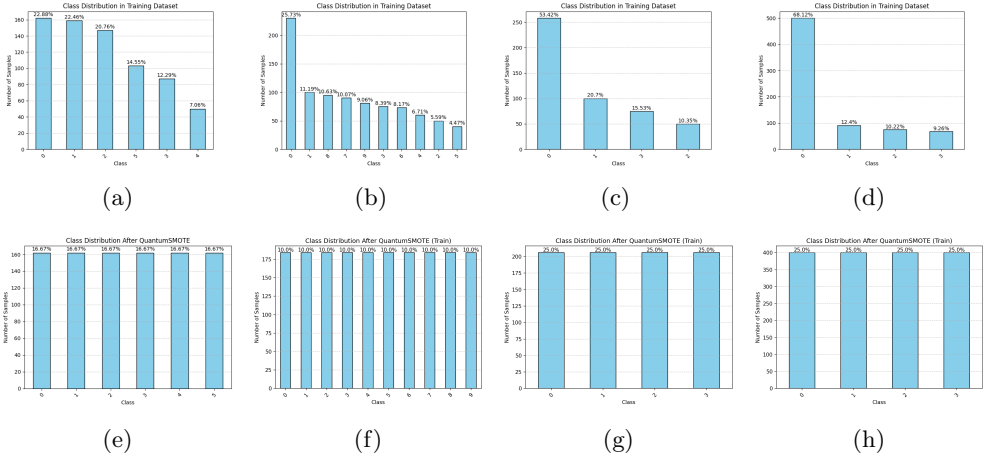


Fig. 3: Distribution of (a) SPID, (b) CWRUBD, (c) EFDD, (d) IFDD before QSMOTE. Distribution of (e) SPID, (f) CWRUBD, (g) EFDD, (h) IFDD after QSMOTE.

The final state is given by

$$\zeta = E_0 \rho E_0^\dagger + E_1 \rho E_1^\dagger. \quad (27)$$

6) Phase Damping Noise: PD captures the loss of quantum coherence without energy dissipation. The Kraus operators are given by

$$E_0 = |0\rangle\langle 0| + \sqrt{1 - \lambda_P} |1\rangle\langle 1|, \quad E_1 = \sqrt{\lambda_P} |1\rangle\langle 1|, \quad (28)$$

where λ_P denotes the PD probability. The noisy evolution is

$$\zeta = E_0 \rho E_0^\dagger + E_1 \rho E_1^\dagger. \quad (29)$$

4.6 Results and Analysis

Fig. 3 depicts the comparative class distributions of the datasets before and after applying the QSMOTE. The subfigures (a)–(d) illustrate the original imbalanced distributions for four datasets: (a) SPID, (b) CWRUBD, (c) EFDD, and (d) IFDD. In each case, certain classes contain substantially fewer samples than others, revealing a pronounced class imbalance that can hinder the performance of classical ML algorithms due to biased learning toward majority classes. Subfigures (e)–(h) show the relevant class distributions after applying QSMOTE. The minority classes are synthetically augmented to obtain a balanced representation in comparison to the majority classes. Comparing the two sets of subfigures demonstrates that QSMOTE effectively equalizes class frequencies across all datasets, resulting in a more uniform distribution. This balanced data structure is expected to improve model generalization, enhance metric stability, and mitigate the bias observed during training on the original imbalanced datasets. The results in Table 1 show that QSMOTE improves

Table 1: Performance Metrics of Classical Algorithms Before and After QSMOTE for Hexa Classification on SPID

Algorithm	Accuracy	Precision	Recall	F1 Measure
Before QSMOTE				
LR	0.7880 ± 0.0342	0.7976 ± 0.0293	0.7880 ± 0.0342	0.7881 ± 0.0313
RF	0.7756 ± 0.0259	0.7847 ± 0.0259	0.7756 ± 0.0259	0.7726 ± 0.0257
SVM	0.8057 ± 0.0200	0.8197 ± 0.0180	0.8057 ± 0.0200	0.8024 ± 0.0223
NB	0.7298 ± 0.0403	0.7465 ± 0.0384	0.7298 ± 0.0403	0.7294 ± 0.0404
DT	0.5724 ± 0.0303	0.5760 ± 0.0278	0.5724 ± 0.0303	0.5677 ± 0.0297
After QSMOTE				
LR	0.8198 ± 0.0076	0.8255 ± 0.0101	0.8198 ± 0.0076	0.8201 ± 0.0095
RF	0.8533 ± 0.0147	0.8556 ± 0.0152	0.8533 ± 0.0147	0.8526 ± 0.0143
SVM	0.8893 ± 0.0149	0.8927 ± 0.0136	0.8893 ± 0.0149	0.8896 ± 0.0145
NB	0.7593 ± 0.0301	0.7659 ± 0.0303	0.7593 ± 0.0301	0.7592 ± 0.0298
DT	0.7439 ± 0.0184	0.7421 ± 0.0206	0.7439 ± 0.0184	0.7393 ± 0.0193

Table 2: Performance Metrics of Classical Algorithms Before and After QSMOTE for Deca-Class Classification on CWRUBD

Algorithm	Accuracy	Precision	Recall	F1 Measure
Before QSMOTE				
LR	0.8783 ± 0.0163	0.8815 ± 0.0319	0.8783 ± 0.0163	0.8654 ± 0.0209
RF	0.9483 ± 0.0241	0.9511 ± 0.0243	0.9483 ± 0.0241	0.9477 ± 0.0245
SVM	0.8797 ± 0.0174	0.8745 ± 0.0247	0.8797 ± 0.0174	0.8664 ± 0.0169
NB	0.9245 ± 0.0168	0.9303 ± 0.0171	0.9245 ± 0.0168	0.9229 ± 0.0170
DT	0.9077 ± 0.0174	0.9152 ± 0.0176	0.9077 ± 0.0174	0.9072 ± 0.0193
After QSMOTE				
LR	0.9332 ± 0.0066	0.9350 ± 0.0068	0.9332 ± 0.0066	0.9328 ± 0.0069
RF	0.9848 ± 0.0044	0.9856 ± 0.0037	0.9848 ± 0.0044	0.9848 ± 0.0044
SVM	0.9522 ± 0.0059	0.9528 ± 0.0063	0.9522 ± 0.0059	0.9518 ± 0.0062
NB	0.8875 ± 0.0182	0.9002 ± 0.0162	0.8875 ± 0.0182	0.8856 ± 0.0196
DT	0.9750 ± 0.0080	0.9764 ± 0.0062	0.9750 ± 0.0080	0.9749 ± 0.0079

the performance of all classical algorithms for the hexa classification task of SPID. Before resampling, SVM gives the best accuracy of 0.8057, followed by LR at 0.7880 and RF at 0.7756, while DT gives the weakest result at only 0.5724. After applying QSMOTE, every model shows clear improvement: LR rises to 0.8198, RF increases to 0.8533, and SVM achieves the highest accuracy of 0.8893. DT also improves notably from 0.5724 to 0.7439, showing that class balancing strongly helps weaker models. NB shows a smaller change, moving from 0.7298 to 0.7593, but still becomes more stable. Overall, QSMOTE balances the data and gives consistent gains in accuracy, precision, recall, and F1-score, with SVM and RF emerging as the best performers. The results

Table 3: Performance Metrics of Classical Algorithms Before and After QSMOTE for Tetra-Class Classification on EFDD

Algorithm	Accuracy	Precision	Recall	F1 Measure
Before QSMOTE				
LR	0.5337 \pm 0.0024	0.3003 \pm 0.0285	0.5337 \pm 0.0024	0.3765 \pm 0.0083
RF	0.4923 \pm 0.0201	0.3403 \pm 0.0788	0.4923 \pm 0.0201	0.3664 \pm 0.0147
SVM	0.5337 \pm 0.0024	0.2848 \pm 0.0026	0.5337 \pm 0.0024	0.3714 \pm 0.0028
NB	0.5156 \pm 0.0113	0.2956 \pm 0.0274	0.5156 \pm 0.0113	0.3681 \pm 0.0090
DT	0.2979 \pm 0.0172	0.3140 \pm 0.0287	0.2979 \pm 0.0172	0.3036 \pm 0.0192
After QSMOTE				
LR	0.2622 \pm 0.0213	0.2582 \pm 0.0232	0.2622 \pm 0.0213	0.2573 \pm 0.0224
RF	0.9126 \pm 0.0259	0.9142 \pm 0.0254	0.9126 \pm 0.0259	0.9116 \pm 0.0263
SVM	0.6420 \pm 0.0226	0.6400 \pm 0.0202	0.6420 \pm 0.0226	0.6358 \pm 0.0207
NB	0.3362 \pm 0.0221	0.3373 \pm 0.0233	0.3362 \pm 0.0221	0.3353 \pm 0.0224
DT	0.8228 \pm 0.0115	0.8266 \pm 0.0159	0.8228 \pm 0.0115	0.8050 \pm 0.0150

Table 4: Performance Metrics of Classical Algorithms Before and After QSMOTE for Tetra-Class Classification on IFDD

Algorithm	Accuracy	Precision	Recall	F1 Measure
Before QSMOTE				
LR	0.6712 \pm 0.0118	0.4728 \pm 0.0222	0.6712 \pm 0.0118	0.5505 \pm 0.0096
RF	0.6763 \pm 0.0089	0.4825 \pm 0.0416	0.6763 \pm 0.0089	0.5527 \pm 0.0108
SVM	0.6814 \pm 0.0028	0.4644 \pm 0.0039	0.6814 \pm 0.0028	0.5523 \pm 0.0037
NB	0.3477 \pm 0.0908	0.4800 \pm 0.0215	0.3477 \pm 0.0908	0.3680 \pm 0.0820
DT	0.4685 \pm 0.0643	0.4912 \pm 0.0467	0.4685 \pm 0.0643	0.4769 \pm 0.0557
After QSMOTE				
LR	0.4450 \pm 0.0109	0.4331 \pm 0.0092	0.4450 \pm 0.0109	0.4352 \pm 0.0092
RF	0.9919 \pm 0.0032	0.9920 \pm 0.0031	0.9919 \pm 0.0032	0.9918 \pm 0.0032
SVM	0.8550 \pm 0.0240	0.8540 \pm 0.0262	0.8550 \pm 0.0240	0.8498 \pm 0.0237
NB	0.4475 \pm 0.0306	0.4476 \pm 0.0333	0.4475 \pm 0.0306	0.4417 \pm 0.0305
DT	0.9006 \pm 0.0111	0.9122 \pm 0.0100	0.9006 \pm 0.0111	0.8916 \pm 0.0134

in Table 2 show that QSMOTE consistently improves the performance of most classifiers on the deca-class dataset of CWRUBD. For LR, the accuracy rises from 0.8783 to 0.9332, with precision increasing from 0.8815 to 0.9350, recall from 0.8783 to 0.9332, and F1-score from 0.8654 to 0.9328. RF achieves the highest performance, as accuracy improves from 0.9483 to 0.9848, and all other metrics exceed 0.984. Similarly, SVM improves in accuracy from 0.8797 to 0.9522, and in F1-score from 0.8664 to 0.9518. In contrast, NB shows a decline after QSMOTE, with accuracy dropping from 0.9245 to 0.8875 and F1-score decreasing from 0.9229 to 0.8856, indicating possible oversensitivity to oversampling. DT benefits substantially, with accuracy increasing from 0.9077

to 0.9750, and F1-score improving from 0.9072 to 0.9749. Overall, QSMOTE improves categorization across most models, with RF and DT performing near-optimally.

Table 3 for EFDD demonstrates that class imbalance severely limited performance prior to resampling, with LR and SVM both at an accuracy of 0.5337 (precision 0.3003 and 0.2848, respectively), RF at 0.4923, NB at 0.5156, and DT markedly lower at 0.2979. After applying QSMOTE, there is a pronounced divergence across model families: RF achieves the best overall performance with accuracy 0.9126, precision 0.9142, recall 0.9126, and F1 0.9116, corresponding to an absolute accuracy gain of +0.4203 (relative \approx 85.4%) over its pre-QSMOTE baseline. DT rises to 0.8228 accuracy (F1 0.8050), an absolute improvement of +0.5249 (relative \approx 176.2%). SVM improves more moderately to 0.6420 accuracy (absolute +0.1083, relative \approx 20.3%). In contrast, LR and NB deteriorate post-QSMOTE (LR to 0.2622, absolute -0.2715 , relative $\approx -50.9\%$; NB to 0.3362, absolute -0.1794 , relative $\approx -34.8\%$), indicating that oversampling benefited non-linear, tree-based methods substantially while offering limited or negative returns for linear/generative models under these features and class overlaps. Table 4 quantitatively compares the performance of classical classifiers before and after applying QSMOTE for IFDD. Before QSMOTE, the highest accuracy is achieved by the SVM classifier (0.6814), followed closely by RF (0.6763) and LR (0.6712). DT and NB perform relatively poorly with accuracies of 0.4685 and 0.3477, respectively. After applying QSMOTE, a significant improvement is observed across most classifiers, especially RF and DT, which attained accuracies of 0.9919 and 0.9006, respectively. The SVM also show a considerable gain to 0.8550, while LR and NB experience marginal changes, with accuracies of 0.4450 and 0.4475, respectively. In terms of overall enhancement, RF exhibits an impressive +46.7% point increase in accuracy, and DT improves by +43.2 points, confirming their ability to leverage balanced samples effectively. The SVM improves by +17.4 points, but the LR and NB decrease by about -22.6 and -10.0 points, respectively. Oversampling is particularly effective for ensemble and tree-based models, resulting in near-perfect classification performance. Linear and probabilistic models are nonetheless susceptible to synthetic class distributions.

4.7 Noisy Results

Fig. 4 presents the classification accuracy of five ML models under varying strengths of six quantum noise channels. Across all noise types, BF, PF, BPF, DP, AD, and PD, SVM remains the most robust, consistently achieving 0.87–0.89 accuracy even at the highest noise probability, with fluctuations below 2–3%. RF and LR show moderate stability, maintaining accuracy around 0.82–0.86, with only minor degradation (< 3%) as noise increases. In contrast, NB and DT exhibit strong sensitivity to noise, often dropping to 0.72–0.76 under severe conditions, particularly for DP and damping noise. Among all noise types, DP noise produces the highest overall degradation (4%), whereas PD has the least impact, especially on SVM and RF. Overall, the results demonstrate that margin-based models (SVM) and ensemble methods (RF) maintain strong discriminative capability under noise, while simpler probabilistic or tree-based models degrade significantly with increasing quantum corruption. The noisy-evaluation plots for the CWRUBD (Fig. 5) show that classical ML models

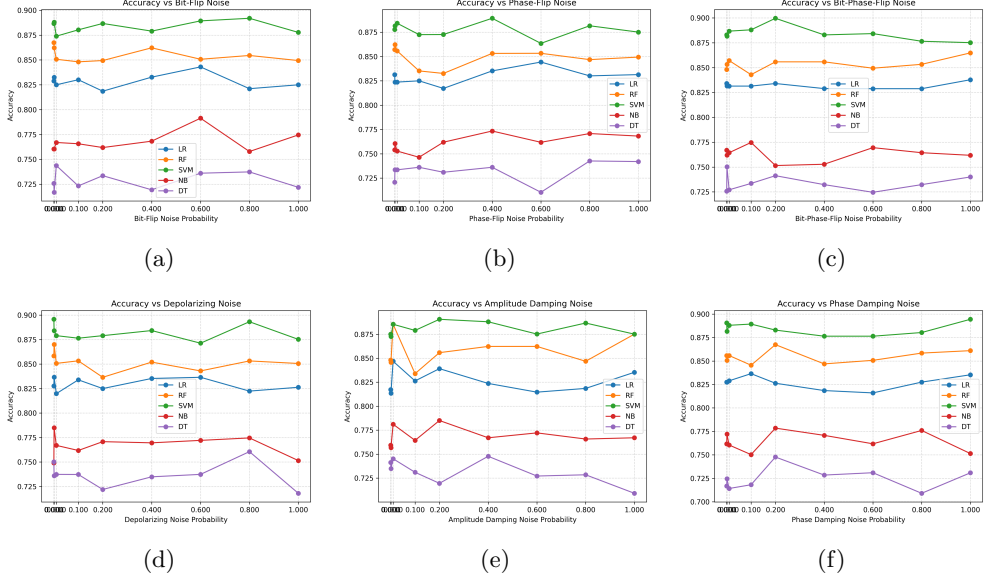


Fig. 4: Noisy results of SPID. a) BF, b) PF, c) BPF, d) DP, e) AD, and f) PD.

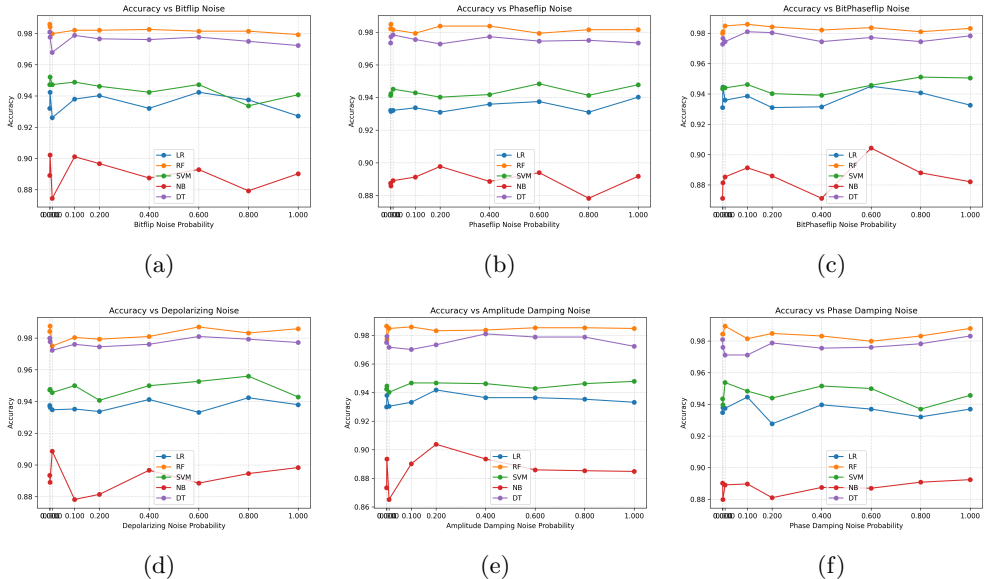


Fig. 5: Noisy results of CWRUBD. a) BF, b) PF, c) BPF, d) DP, e) AD, and f) PD.

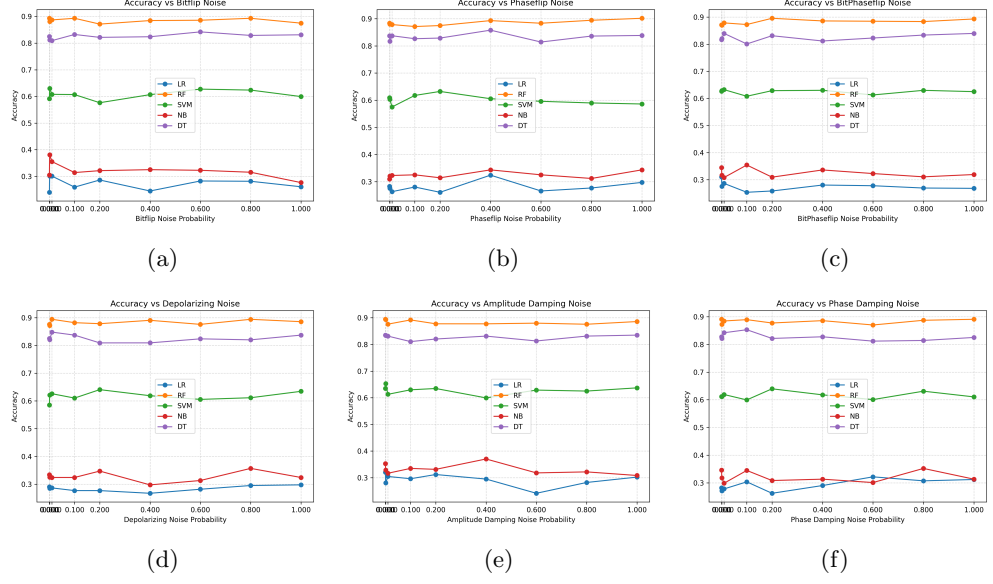


Fig. 6: Noisy results of EFDD. a) BF, b) PF, c) BPF, d) DP, e) AD, and f) PD.

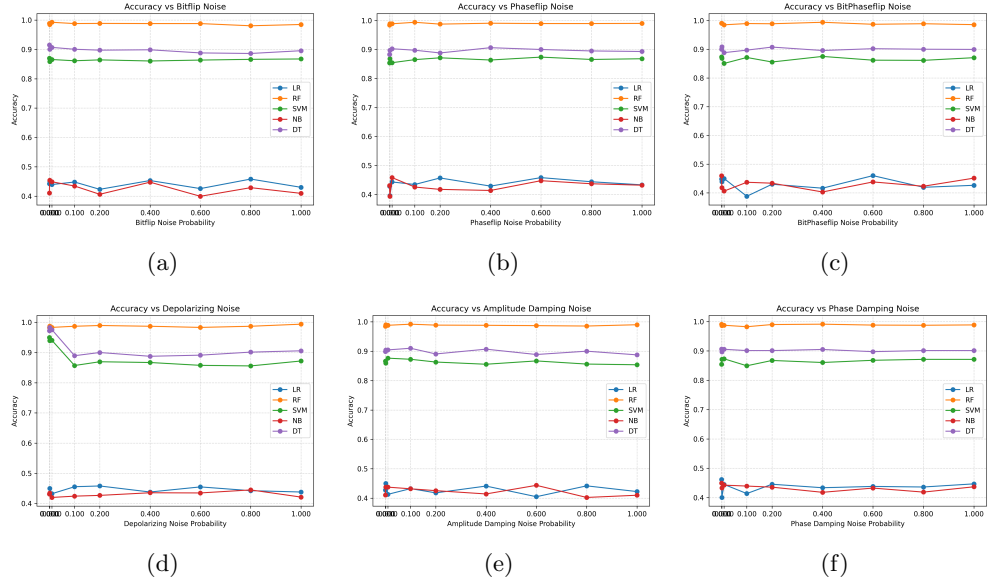


Fig. 7: Noisy results of IFDD. a) BF, b) PF, c) BPF, d) DP, e) AD, and f) PD.

exhibit high robustness across all six quantum-noise channels, BF, PF, BPF, DP, AD, and PD, although the degree of stability varies by algorithm. RF and DT consistently achieve the highest accuracies in the range of 0.96–0.99, with minimal degradation (< 0.01) even when noise probability increases to 1.0, indicating strong invariance to stochastic disturbances. SVM and LR maintain moderate robustness, staying between 0.92–0.95, with slight oscillations as noise increases. NB shows noticeable sensitivity, fluctuating between 0.88–0.91, especially under BF and BPF noise, where sharp drops of 0.02–0.03 occur at intermediate noise levels.

Fig. 6 presents the robustness analysis of five classical classifiers, LR, RF, SVM, NB, and DT under increasing levels of six quantum noise models on the EFDD: BF, PF, BPF, DP, AD, and PD. Across all noise types, RF consistently achieves the highest accuracy (≈ 0.88 –0.90), showing minimal degradation even at maximum noise probability. Next, DT fluctuates around 0.8 accuracy. SVM forms a mid-tier cluster with accuracies around 0.68–0.70, remaining nearly noise-insensitive. NB and LR perform poorly, with NB ranging between 0.30–0.35 and DT sharply varying between 0.25–0.32 depending on noise type. Overall, RF is the most noise-robust model on EFDD, while NB and LR degrade significantly, confirming that EFDD is highly noise-sensitive for weak, variance-prone learners. Fig. 7 illustrates how five classical ML models, LR, RF, SVM, NB, and DT, perform under increasing levels of quantum noise injected into the IFDD dataset. Across all six noise channels (BF, PF, BPF, DP, AD, and PD), RF consistently achieves the highest accuracy, remaining close to 0.95–0.99 even at maximum noise probability, demonstrating strong robustness. SVM and DT maintain stable performance (≈ 0.80 –0.90) across all noise types, showing only minor fluctuations ($< 3\%$) as noise increases. NB and LR exhibit the lowest and most unstable accuracy, often dropping to ≈ 0.40 –0.50 depending on the noise model. A general pattern across all subplots is that RF and SVM exhibit negligible degradation even when noise probability hits 1.0, demonstrating their robustness to quantum noise perturbations. In contrast, NB and LR decrease strongly across all noise types, demonstrating a high vulnerability.

4.8 Discussion

Fig. 3 and Tables 1–4 collectively highlight the impact of the QSMOTE on mitigating class imbalance across multiple datasets (SPID, CWRUBD, EFDD, and IFDD) and classification complexities (hexa-, deca-, tetra-, and tetra-class setups). The visual evidence in Fig. 3 demonstrates that QSMOTE effectively reconstructs class distributions, equalizing the minority and majority samples to create a uniform representation. This structural balance significantly improves the learning capability of most classical models by reducing bias toward dominating classes and allowing for improved generalization. Across all datasets, quantitative results consistently show a significant improvement in performance following QSMOTE application. Accuracy in SPID (hexa classification) improves significantly for all models, with SVM increasing from 0.8057 to 0.8893 and RF from 0.7756 to 0.8533, while precision, recall, and F1-score remain consistent. In CWRUBD (deca-class classification), RF and DT emerge as the most important beneficiaries, achieving 0.9848 and 0.9750 accuracy, respectively, illustrating the capacity of ensemble and tree-based algorithms to successfully use

the synthetic balance created by QSMOTE. Similarly, in EFDD (tetra-class classification), RF demonstrates a substantial boost from 0.4923 to 0.9126 accuracy, while DT rises from 0.2979 to 0.8228, indicating over 80-170% relative improvement. IFDD (tetra-class classification) follows this trend, with RF achieving near-perfect accuracy of 0.9919 and DT reaching 0.9006 following QSMOTE, demonstrating that tree-based learners handle oversampled distributions quite well.

However, not every model benefits equally. Linear classifiers such as LR and probabilistic models like NB may perform poorly (e.g., LR in EFDD dropped from 0.5337 to 0.2622), showing that synthetic interpolation may distort feature boundaries when linear separability assumptions fail. This suggests that QSMOTE's interpolation technique may sometimes oversimplify or misrepresent high-dimensional feature interactions, particularly in datasets with overlapping minority and majority class regions. Nonetheless, the continuous performance improvement for RF, DT, and SVM demonstrates QSMOTE's utility in supporting non-linear decision surfaces. Overall, the comparison analysis shows that QSMOTE significantly improves classification stability and accuracy across most datasets by correcting for imbalance-induced bias. The top-performing models, RF and DT, attain near-optimal precision, recall, and F1-score consistency, demonstrating that balanced sampling combined with ensemble learning is a reliable solution for complicated, multi-class intrusion detection problems. These findings provide a solid foundation for evaluating more advanced resampling frameworks like quantum-inspired balancing, which seek to improve minority class representation while maintaining feature-space fidelity.

The noisy-evaluation results shown in Fig. 4–7 provide a detailed assessment of the robustness of classical ML models under multiple quantum-inspired noise channels, namely BF, PF, BPF, DP, AD, and PD, across four fault-diagnostic datasets. On the SPID (Fig. 4), SVM consistently emerges as the most noise-resilient classifier, maintaining high accuracy even at extreme noise levels with only marginal fluctuations. RF and LR also demonstrate stable behavior, with only minor performance degradation as noise strength increases. In contrast, NB and DT exhibit pronounced sensitivity, particularly under depolarizing and damping noise, which introduce the strongest corruption effects. Among the noise models, depolarizing noise has the most disruptive impact overall, while phase-damping noise proves to be the least harmful, especially for margin-based and ensemble learners. These findings suggest that classifiers based on global margin optimization or ensemble averaging are fundamentally more resilient to random perturbations in this dataset. The CWRUBD (Fig. 5) shows that all classical models are significantly more resilient than SPID, indicating the data's inherent separability. RF and DT attain near-saturated accuracy across all noise channels, demonstrating nearly full invariance even at the highest noise probability. SVM and LR retain continuously excellent performance with relatively minor oscillations, whereas NB shows significant susceptibility to BF and BPF noise. Overall, the findings indicate that CWRUBD is less susceptible to quantum-inspired noise, and that both ensemble and linear classifiers may effectively maintain discriminative structure despite extreme perturbations.

The robustness trends vary significantly for the EFDD (Fig. 6), as model separation gets more pronounced. RF once again displays superior stability across all

noise types, showing its robustness in more difficult environments. DT maintains moderate accuracy but is more variable, whereas SVM falls into a relatively steady mid-performance category with low noise sensitivity. In contrast, NB and LR experience significant degradation, with accuracy reducing dramatically across most noise channels. These findings suggest that EFDD is fundamentally more noise-sensitive, especially for variance-prone and probabilistic models, and that model capacity and ensemble diversity are crucial in reducing quantum-induced disturbances. A similar but more pronounced pattern is evident on the IFDD (Fig. 7). RF consistently gives the maximum accuracy across all noise channels, with low degradation even at high noise levels, demonstrating its resilience. SVM and DT maintain consistent mid-range performance, whereas NB and LR exhibit the lowest and most unstable accuracy, with substantial drops across all noise models. The persistence of these trends across datasets reveals a common pattern: ensemble methods and margin-based classifiers are significantly more resistant to quantum noise, whereas simpler probabilistic and linear models are highly corruptible, especially in datasets with higher complexity and class overlap. Overall, the results from all four datasets show that RF and SVM are the most resilient against quantum-inspired noise, maintaining constant performance even under extreme perturbations. In contrast, NB and LR show significant vulnerability, particularly in noise-sensitive datasets like EFDD and IFDD. These findings underline the need of using noise-tolerant models, particularly ensemble and margin-based techniques, when deploying ML systems in situations with quantum noise or high uncertainty.

5 Conclusion

This study provided a detailed evaluation of classical ML models from two complementary perspectives that are critical for industrial defect diagnosis: (i) class imbalance reduction using QSMOTE and (ii) robustness assessment under quantum-inspired noise. The experimental results across four benchmark datasets SPID, CWRUBD, EFDD, and IFDD and multiple multi-class configurations demonstrate that data imbalance and quantum-level noise have significant and distinct impacts on classifier performance. First, the QSMOTE analysis (Fig. 3 and Tables 1–4) shows that oversampling strongly enhances the representational fidelity of minority classes, creating more uniform training distributions. This structural rebalancing leads to substantial gains in accuracy, precision, recall, and F1-score across most classical models and datasets. RF, DT, and SVM consistently experience the most pronounced improvement e.g., SVM on SPID rising from 0.8057 to 0.8893, RF on EFDD jumping from 0.4923 to 0.9126, and DT on IFDD improving from 0.7393 to 0.9006 indicating that non-linear learners benefit most from enriched minority-class manifolds. However, linear and probabilistic classifiers occasionally degrade after QSMOTE (e.g., LR on EFDD), illustrating that synthetic interpolation may distort linear decision boundaries in highly overlapping feature spaces. Thus, while QSMOTE reliably enhances ensemble and kernel-based models, its effectiveness remains model- and dataset-dependent.

This work investigated the robustness of classical ML classifiers under multiple quantum-inspired noise channels, including BF, PF, BPF, DP, AD, and PD noise,

across four fault-diagnostic datasets. The experimental results consistently demonstrate that ensemble-based and margin-based models exhibit superior resilience to noise-induced perturbations. Even in extreme noise environments, RF and SVM classifiers maintain good classification accuracy, demonstrating their intrinsic tolerance to stochastic corruption and uncertainty. In contrast, probabilistic and simpler linear models, like as NB and LR, exhibit significant performance loss, particularly on datasets with high complexity and class overlap. The investigation also shows that dataset properties have an important impact in influencing noise sensitivity. While datasets with higher intrinsic separability, such as CWRUBD, are mostly unaffected by extreme noise, more difficult datasets, such as EFDD and IFDD, increase the sensitivity of variance-prone learners. Across all datasets, DP noise is the most disruptive channel, with phase-damping noise having the least impact on classification performance. These findings highlight the need of using noise-tolerant model designs for deploying ML systems in quantum-noisy or unpredictable situations. Overall, the findings offer useful recommendations for robust model selection and establish solid classical baselines for future comparisons with quantum and quantum-inspired learning approaches.

Supplementary information. The supplementary information is provided in the Appendix section [A](#).

Declarations

- Funding: Authors declare that there has been no external funding.
- Conflict of interest/Competing interests: The authors have no financial or non-financial competing interests.
- Data and Materials Availability: All the data used in this manuscript are provided with URL links, which can be easily accessed.
- Author contribution: The authors confirm their contribution to the paper as follows: Study conception, design and methodology: A.S.P., H.R.P., B.K.B.; Data collection: A.S.P.; Analysis and interpretation of results: A.S.P., H.R.P., B.K.B.; Draft manuscript preparation: A.S.P., H.R.P., B.K.B.; Supervision: H.R.P.; All authors reviewed the results and approved the final version of the manuscript.

Appendix A Supplementary Material

The sample distribution for Solar Panel Image Dataset (SPID) before and after Synthetic Minority Oversampling Technique (SMOTE) is shown in Figs. [A1](#) and [A2](#). The results in Table [A1](#) show that QSMOTE improves the performance of all classical algorithms in binary classification. Before resampling, logistic regression (LR) gives the best accuracy of 0.9344, followed by support vector machine (SVM) (0.9103) and random forest (RF) (0.8802). Decision tree (DT) shows the weakest result at 0.8205, while naive bayes (NB) stays moderate at 0.8813. After applying QSMOTE, every model performs better. RF gives the highest accuracy of 0.9804, precision of 0.9822, recall of 0.9804, and F1-score of 0.9803. SVM follows with 0.9764 accuracy and F1-score of 0.9762, showing strong balance across metrics. LR also improves to 0.9685

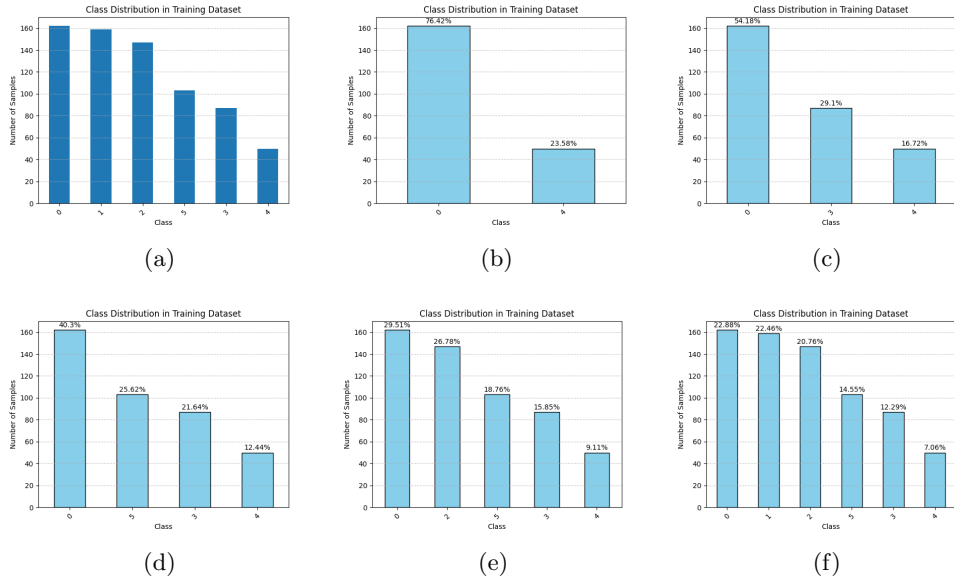


Fig. A1: (a) Initial Distribution of SPID. Class Percentages in (b) Binary, (c) Tertiary, (d) Tetra, (e) Penta, and (f) Hexa Classification Before QSMOTE.

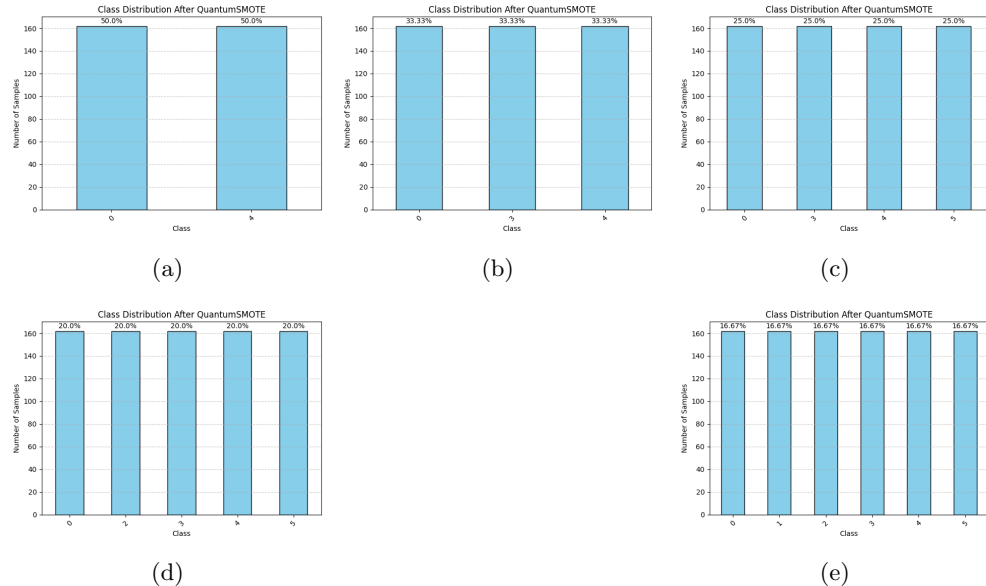


Fig. A2: Final Distribution of SPID. Class Percentages in (b) Binary, (c) Tertiary, (d) Tetra, (e) Penta, and (f) Hexa Classification After QSMOTE.

Table A1: Performance Metrics of Classical Algorithms Before and After QSMOTE for Binary Classification on SPID

Algorithm	Accuracy	Precision	Recall	F1 Measure
Before QSMOTE				
LR	0.9344 ± 0.0285	0.9348 ± 0.0302	0.9344 ± 0.0285	0.9324 ± 0.0305
RF	0.8802 ± 0.0192	0.8930 ± 0.0159	0.8802 ± 0.0192	0.8657 ± 0.0260
SVM	0.9103 ± 0.0263	0.9204 ± 0.0211	0.9103 ± 0.0263	0.9013 ± 0.0319
NB	0.8813 ± 0.0760	0.8815 ± 0.0787	0.8813 ± 0.0760	0.8749 ± 0.0792
DT	0.8205 ± 0.0496	0.8213 ± 0.0585	0.8205 ± 0.0496	0.8168 ± 0.0524
After QSMOTE				
LR	0.9685 ± 0.0200	0.9711 ± 0.0179	0.9685 ± 0.0200	0.9685 ± 0.0200
RF	0.9804 ± 0.0248	0.9822 ± 0.0224	0.9804 ± 0.0248	0.9803 ± 0.0249
SVM	0.9764 ± 0.0380	0.9798 ± 0.0316	0.9764 ± 0.0380	0.9762 ± 0.0383
NB	0.8900 ± 0.0338	0.9055 ± 0.0277	0.8900 ± 0.0338	0.8887 ± 0.0348
DT	0.9016 ± 0.0277	0.9082 ± 0.0285	0.9016 ± 0.0277	0.9012 ± 0.0278

Table A2: Performance Metrics of Classical Algorithms Before and After QSMOTE for Tertiary Classification on SPID

Algorithm	Accuracy	Precision	Recall	F1 Measure
Before QSMOTE				
LR	0.8159 ± 0.0278	0.8194 ± 0.0240	0.8159 ± 0.0278	0.8132 ± 0.0267
RF	0.8577 ± 0.0244	0.8690 ± 0.0242	0.8577 ± 0.0244	0.8480 ± 0.0284
SVM	0.8618 ± 0.0290	0.8734 ± 0.0352	0.8618 ± 0.0290	0.8469 ± 0.0333
NB	0.8325 ± 0.0377	0.8333 ± 0.0399	0.8325 ± 0.0377	0.8248 ± 0.0437
DT	0.7746 ± 0.0669	0.7956 ± 0.0652	0.7746 ± 0.0669	0.7778 ± 0.0627
After QSMOTE				
LR	0.8531 ± 0.0191	0.8544 ± 0.0204	0.8531 ± 0.0191	0.8528 ± 0.0188
RF	0.9458 ± 0.0387	0.9474 ± 0.0384	0.9458 ± 0.0387	0.9455 ± 0.0391
SVM	0.9535 ± 0.0158	0.9561 ± 0.0142	0.9535 ± 0.0158	0.9536 ± 0.0157
NB	0.8427 ± 0.0502	0.8494 ± 0.0508	0.8427 ± 0.0502	0.8402 ± 0.0508
DT	0.8890 ± 0.0367	0.8946 ± 0.0298	0.8890 ± 0.0367	0.8887 ± 0.0361

accuracy and F1-score. Weaker models also gain. DT increases from 0.8205 to 0.9016 accuracy (about 10% gain) and F1-score of 0.9012, while NB improves from 0.8813 to 0.8900 accuracy with F1-score of 0.8887. Overall, QSMOTE boosts both strong models (RF, SVM, LR) and weaker models (DT, NB). RF shows the best performance after resampling, while SVM and LR also stay highly effective. The results in Table A2 show that QSMOTE improves all classical algorithms for tertiary classification. Before resampling, SVM gives the highest accuracy of 0.8618, followed by RF (0.8577) and NB (0.8325), while LR (0.8159) and DT (0.7746) perform lower. After QSMOTE, every model improves. SVM reaches 0.9535 accuracy and 0.9536 F1-score, and RF achieves 0.9458 accuracy with F1 0.9455, showing strong performance. LR rises to

Table A3: Performance Metrics of Classical Algorithms Before and After QSMOTE for Tetra Classification on SPID

Algorithm	Accuracy	Precision	Recall	F1 Measure
Before QSMOTE				
LR	0.8504 \pm 0.0380	0.8554 \pm 0.0416	0.8504 \pm 0.0380	0.8492 \pm 0.0389
RF	0.8597 \pm 0.0579	0.8699 \pm 0.0675	0.8597 \pm 0.0579	0.8534 \pm 0.0628
SVM	0.8785 \pm 0.0348	0.8912 \pm 0.0425	0.8785 \pm 0.0348	0.8692 \pm 0.0375
NB	0.8287 \pm 0.0310	0.8352 \pm 0.0345	0.8287 \pm 0.0310	0.8243 \pm 0.0340
DT	0.7632 \pm 0.0391	0.7714 \pm 0.0388	0.7632 \pm 0.0391	0.7625 \pm 0.0384
After QSMOTE				
LR	0.9016 \pm 0.0421	0.9018 \pm 0.0430	0.9016 \pm 0.0421	0.9006 \pm 0.0430
RF	0.9421 \pm 0.0086	0.9438 \pm 0.0075	0.9421 \pm 0.0086	0.9421 \pm 0.0086
SVM	0.9479 \pm 0.0208	0.9494 \pm 0.0203	0.9479 \pm 0.0208	0.9478 \pm 0.0210
NB	0.8456 \pm 0.0120	0.8566 \pm 0.0128	0.8456 \pm 0.0120	0.8451 \pm 0.0127
DT	0.8881 \pm 0.0271	0.8904 \pm 0.0271	0.8881 \pm 0.0271	0.8868 \pm 0.0268

Table A4: Performance Metrics of Classical Algorithms Before and After QSMOTE for Penta Classification on SPID

Algorithm	Accuracy	Precision	Recall	F1 Measure
Before QSMOTE				
LR	0.7835 \pm 0.0384	0.7887 \pm 0.0393	0.7835 \pm 0.0384	0.7823 \pm 0.0366
RF	0.7722 \pm 0.0259	0.7795 \pm 0.0290	0.7722 \pm 0.0259	0.7690 \pm 0.0258
SVM	0.8176 \pm 0.0331	0.8305 \pm 0.0277	0.8176 \pm 0.0331	0.8143 \pm 0.0330
NB	0.7835 \pm 0.0343	0.7908 \pm 0.0338	0.7835 \pm 0.0343	0.7810 \pm 0.0363
DT	0.6263 \pm 0.0448	0.6355 \pm 0.0425	0.6263 \pm 0.0448	0.6250 \pm 0.0410
After QSMOTE				
LR	0.8364 \pm 0.0286	0.8425 \pm 0.0277	0.8364 \pm 0.0286	0.8380 \pm 0.0279
RF	0.8811 \pm 0.0250	0.8831 \pm 0.0254	0.8811 \pm 0.0250	0.8801 \pm 0.0259
SVM	0.8796 \pm 0.0235	0.8837 \pm 0.0223	0.8796 \pm 0.0235	0.8800 \pm 0.0235
NB	0.7870 \pm 0.0132	0.7954 \pm 0.0127	0.7870 \pm 0.0132	0.7876 \pm 0.0115
DT	0.7778 \pm 0.0195	0.7784 \pm 0.0194	0.7778 \pm 0.0195	0.7708 \pm 0.0198

0.8531 accuracy and F1 0.8528, and DT increases from 0.7746 to 0.8890 in accuracy, with F1 0.8887, showing the highest relative improvement. NB also improves modestly to 0.8427 accuracy and F1 0.8402. Overall, QSMOTE balances the classes and boosts both strong models (SVM, RF) and weaker models (LR, DT, NB), giving consistent gains across accuracy, precision, recall, and F1.

The results in Table A3 highlight the quantitative impact of QSMOTE on tetra classification performance. Prior to resampling, SVM achieves the best accuracy at 0.8785, followed by RF at 0.8597 and LR at 0.8504, whereas DT performs the weakest with an accuracy of only 0.7632. After applying QSMOTE, all models record substantial improvements: SVM rises to 0.9479 (a gain of nearly +7%), RF reaches 0.9421 (an

increase of about +8%), and LR improves to 0.9016 (a gain of around +5%). DT also exhibits remarkable progress, moving from 0.7632 to 0.8881, representing the highest relative improvement of approximately +16%. NB, while showing the smallest absolute change, still improves from 0.8287 to 0.8456. Similar upward trends are observed across precision, recall, and F1-measure, with SVM and RF consistently achieving the strongest overall metrics after resampling. These results quantitatively demonstrate that QSMOTE not only boosts average performance but also reduces variability, particularly benefiting weaker learners like DT while further enhancing strong performers such as SVM and RF. The results in Table A4 quantitatively demonstrate the effectiveness of QSMOTE in improving classification performance for the penta-class problem. Before resampling, SVM achieves the highest accuracy of 0.8176, followed by LR and NB at 0.7835, while RF slightly lags at 0.7722 and DT performs the weakest with only 0.6263. After applying QSMOTE, all models exhibit significant gains: RF improves from 0.7722 to 0.8811 (a relative increase of about +14%), SVM rises from 0.8176 to 0.8796 (+7.6%), and LR advances from 0.7835 to 0.8364 (+6.8%). The most dramatic improvement is observed in DT, which jumps from 0.6263 to 0.7778, reflecting a relative gain of nearly +24%, indicating that QSMOTE effectively mitigates its earlier limitations. NB shows the smallest change, moving from 0.7835 to 0.7870, but still gains stability with reduced variance. Consistently across precision, recall, and F1-measure, RF and SVM emerge as the best-performing models post-QSMOTE, underscoring that oversampling not only enhances accuracy but also ensures balanced generalization in complex multi-class settings.

Table A5: Performance Metrics of Classical Algorithms Before and After QSMOTE for Binary Classification on CWRUBD

Algorithm	Accuracy	Precision	Recall	F1 Measure
Before QSMOTE				
LR	0.9887 ± 0.0092	0.9891 ± 0.0089	0.9887 ± 0.0092	0.9886 ± 0.0093
RF	0.9885 ± 0.0153	0.9892 ± 0.0145	0.9885 ± 0.0153	0.9884 ± 0.0156
SVM	0.9962 ± 0.0075	0.9964 ± 0.0071	0.9962 ± 0.0075	0.9963 ± 0.0075
NB	0.9962 ± 0.0075	0.9964 ± 0.0071	0.9962 ± 0.0075	0.9963 ± 0.0075
DT	0.9847 ± 0.0224	0.9858 ± 0.0207	0.9847 ± 0.0224	0.9844 ± 0.0231
After QSMOTE				
LR	0.9946 ± 0.0067	0.9947 ± 0.0065	0.9946 ± 0.0067	0.9946 ± 0.0067
RF	0.9946 ± 0.0066	0.9947 ± 0.0064	0.9946 ± 0.0066	0.9946 ± 0.0066
SVM	0.9946 ± 0.0108	0.9949 ± 0.0103	0.9946 ± 0.0108	0.9946 ± 0.0108
NB	0.9783 ± 0.0108	0.9794 ± 0.0098	0.9783 ± 0.0108	0.9782 ± 0.0108
DT	0.9945 ± 0.0067	0.9947 ± 0.0065	0.9945 ± 0.0067	0.9945 ± 0.0067

The results in Table A5 for CWRU Bearing Dataset (CWRUBD) indicate that all classifiers perform very strongly in the binary classification setting, with minimal variation across models. Before QSMOTE, both SVM and NB achieve the best results, attaining accuracies of 0.9962 ± 0.0075 , precisions of 0.9964 ± 0.0071 , recalls of 0.9962 ± 0.0075 , and F1 scores of 0.9963 ± 0.0075 . LR and RF follow closely with

accuracies around 0.9887 ± 0.0092 and 0.9885 ± 0.0153 , respectively, while DT records the lowest accuracy of 0.9847 ± 0.0224 . After applying QSMOTE, LR and RF improve to 0.9946 ± 0.0067 and 0.9946 ± 0.0066 , respectively, while SVM slightly decreases to 0.9946 ± 0.0108 , showing a marginal drop of about 0.16% compared to its pre-QSMOTE performance. Interestingly, NB exhibits a notable decline after QSMOTE, dropping from 0.9962 ± 0.0075 to 0.9783 ± 0.0108 , highlighting its sensitivity to synthetic oversampling. DT, in contrast, improves significantly, rising from 0.9847 ± 0.0224 to 0.9945 ± 0.0067 , representing an absolute gain of nearly 1.0%. Overall, while most classifiers benefit from QSMOTE, SVM remained the most consistent high performer, whereas NB shows reduced robustness in this binary setting.

Table A6: Performance Metrics of Classical Algorithms Before and After QSMOTE for Tertiary Classification on CWRUBD

Algorithm	Accuracy	Precision	Recall	F1 Measure
Before QSMOTE				
LR	0.9637 ± 0.0165	0.9651 ± 0.0178	0.9637 ± 0.0165	0.9636 ± 0.0172
RF	0.9639 ± 0.0191	0.9657 ± 0.0188	0.9639 ± 0.0191	0.9633 ± 0.0194
SVM	0.9639 ± 0.0191	0.9671 ± 0.0174	0.9639 ± 0.0191	0.9623 ± 0.0202
NB	0.9507 ± 0.0180	0.9558 ± 0.0160	0.9507 ± 0.0180	0.9506 ± 0.0174
DT	0.9442 ± 0.0382	0.9484 ± 0.0361	0.9442 ± 0.0382	0.9439 ± 0.0373
After QSMOTE				
LR	0.9765 ± 0.0072	0.9768 ± 0.0072	0.9765 ± 0.0072	0.9764 ± 0.0072
RF	0.9855 ± 0.0122	0.9861 ± 0.0116	0.9855 ± 0.0122	0.9855 ± 0.0122
SVM	0.9765 ± 0.0157	0.9771 ± 0.0156	0.9765 ± 0.0157	0.9765 ± 0.0157
NB	0.9656 ± 0.0155	0.9665 ± 0.0151	0.9656 ± 0.0155	0.9657 ± 0.0154
DT	0.9729 ± 0.0213	0.9738 ± 0.0203	0.9729 ± 0.0213	0.9728 ± 0.0214

The results in Table A6 demonstrate the effectiveness of QSMOTE in improving tertiary classification performance across most classifiers. Before QSMOTE, LR, RF, and SVM achieve comparable accuracies of 0.9637 ± 0.0165 , 0.9639 ± 0.0191 , and 0.9639 ± 0.0191 , respectively, with SVM attaining the highest precision of 0.9671 ± 0.0174 . NB and DT underperform with accuracies of 0.9507 ± 0.0180 and 0.9442 ± 0.0382 , respectively. After applying QSMOTE, all classifiers exhibit performance gains, with RF again emerging as the best performer, achieving an accuracy of 0.9855 ± 0.0122 , precision of 0.9861 ± 0.0116 , recall of 0.9855 ± 0.0122 , and F1 score of 0.9855 ± 0.0122 . This corresponds to a relative improvement of approximately 2.2% in accuracy compared to its pre-QSMOTE counterpart. LR and SVM also improve to accuracies of 0.9765 ± 0.0072 and 0.9765 ± 0.0157 , respectively, while DT rises markedly from 0.9442 ± 0.0382 to 0.9729 ± 0.0213 , showing a relative gain of nearly 3.0%. NB, although showing a modest increase, improves to 0.9656 ± 0.0155 . Overall, the application of QSMOTE enhances the robustness and balance of classifiers, with RF consistently outperforming all other methods across all evaluation metrics.

The results in Table A7 highlight the quantitative improvements achieved through QSMOTE in the tetra-class classification task. Before resampling, RF attains the best

Table A7: Performance Metrics of Classical Algorithms Before and After QSMOTE for Tetra-Class Classification on CWRUBD

Algorithm	Accuracy	Precision	Recall	F1 Measure
Before QSMOTE				
LR	0.9698 ± 0.0201	0.9706 ± 0.0207	0.9698 ± 0.0201	0.9696 ± 0.0204
RF	0.9781 ± 0.0164	0.9794 ± 0.0153	0.9781 ± 0.0164	0.9773 ± 0.0172
SVM	0.9753 ± 0.0159	0.9781 ± 0.0123	0.9753 ± 0.0159	0.9740 ± 0.0183
NB	0.9588 ± 0.0149	0.9627 ± 0.0121	0.9588 ± 0.0149	0.9589 ± 0.0141
DT	0.9616 ± 0.0201	0.9626 ± 0.0203	0.9616 ± 0.0201	0.9615 ± 0.0202
After QSMOTE				
LR	0.9755 ± 0.0133	0.9762 ± 0.0131	0.9755 ± 0.0133	0.9756 ± 0.0133
RF	0.9918 ± 0.0027	0.9921 ± 0.0027	0.9918 ± 0.0027	0.9918 ± 0.0028
SVM	0.9878 ± 0.0100	0.9882 ± 0.0097	0.9878 ± 0.0100	0.9878 ± 0.0100
NB	0.9497 ± 0.0092	0.9507 ± 0.0093	0.9497 ± 0.0092	0.9497 ± 0.0092
DT	0.9891 ± 0.0033	0.9895 ± 0.0032	0.9891 ± 0.0033	0.9891 ± 0.0034

performance with an accuracy of 0.9781 ± 0.0164 , precision of 0.9794 ± 0.0153 , recall of 0.9781 ± 0.0164 , and F1 score of 0.9773 ± 0.0172 . LR and SVM follow closely with accuracies of 0.9698 ± 0.0201 and 0.9753 ± 0.0159 , respectively, while NB perform the weakest with accuracy 0.9588 ± 0.0149 . After applying QSMOTE, all classifiers except NB demonstrate consistent improvements. RF achieves the highest overall metrics, reaching an accuracy of 0.9918 ± 0.0027 , precision of 0.9921 ± 0.0027 , recall of 0.9918 ± 0.0027 , and F1 score of 0.9918 ± 0.0028 , representing an approximate 1.4% accuracy gain compared to its performance on the imbalanced dataset. SVM and DT also show significant improvements, achieving accuracies of 0.9878 ± 0.0100 and 0.9891 ± 0.0033 , respectively. In contrast, NB experiences a slight decrease in performance after QSMOTE, dropping from 0.9588 ± 0.0149 to 0.9497 ± 0.0092 in accuracy. Overall, QSMOTE proves effective in improving the robustness of most classifiers, particularly RF, which outperformed all other methods across all evaluation metrics.

The results in Table A8 show that QSMOTE consistently improves most classifiers for the penta-class dataset, with the exception of NB. LR improves from an accuracy of 0.9757 ± 0.0204 to 0.9880 ± 0.0063 , with corresponding increases in precision (0.9767 ± 0.0198 to 0.9882 ± 0.0062), recall (0.9757 ± 0.0204 to 0.9880 ± 0.0063), and F1-score (0.9753 ± 0.0208 to 0.9880 ± 0.0063). RF achieves the highest performance, with accuracy rising from 0.9685 ± 0.0122 to 0.9957 ± 0.0041 , and all other metrics exceeding 0.995. Similarly, SVM improves in accuracy from 0.9758 ± 0.0107 to 0.9880 ± 0.0087 , and in F1-score from 0.9751 ± 0.0111 to 0.9880 ± 0.0087 . DT also benefits, with accuracy increasing from 0.9612 ± 0.0140 to 0.9815 ± 0.0027 , and F1-score from 0.9609 ± 0.0141 to 0.9814 ± 0.0026 . In contrast, NB shows a decline, as accuracy drops from 0.9733 ± 0.0142 to 0.9446 ± 0.0121 , and F1-score decreases from 0.9727 ± 0.0153 to 0.9439 ± 0.0124 , indicating oversensitivity to synthetic samples. Overall, QSMOTE strongly boosts LR, RF, SVM, and DT, with RF achieving near-perfect classification, while NB remains adversely affected.

Table A8: Performance Metrics of Classical Algorithms Before and After QSMOTE for Penta-Class Classification on CWRUBD

Algorithm	Accuracy	Precision	Recall	F1 Measure
Before QSMOTE				
LR	0.9757 \pm 0.0204	0.9767 \pm 0.0198	0.9757 \pm 0.0204	0.9753 \pm 0.0208
RF	0.9685 \pm 0.0122	0.9697 \pm 0.0123	0.9685 \pm 0.0122	0.9682 \pm 0.0121
SVM	0.9758 \pm 0.0107	0.9767 \pm 0.0106	0.9758 \pm 0.0107	0.9751 \pm 0.0111
NB	0.9733 \pm 0.0142	0.9736 \pm 0.0156	0.9733 \pm 0.0142	0.9727 \pm 0.0153
DT	0.9612 \pm 0.0140	0.9648 \pm 0.0126	0.9612 \pm 0.0140	0.9609 \pm 0.0141
After QSMOTE				
LR	0.9880 \pm 0.0063	0.9882 \pm 0.0062	0.9880 \pm 0.0063	0.9880 \pm 0.0063
RF	0.9957 \pm 0.0041	0.9958 \pm 0.0039	0.9957 \pm 0.0041	0.9956 \pm 0.0041
SVM	0.9880 \pm 0.0087	0.9882 \pm 0.0086	0.9880 \pm 0.0087	0.9880 \pm 0.0087
NB	0.9446 \pm 0.0121	0.9471 \pm 0.0112	0.9446 \pm 0.0121	0.9439 \pm 0.0124
DT	0.9815 \pm 0.0027	0.9823 \pm 0.0024	0.9815 \pm 0.0027	0.9814 \pm 0.0026

Table A9: Performance Metrics of Classical Algorithms Before and After QSMOTE for Hexa-Class Classification on CWRUBD

Algorithm	Accuracy	Precision	Recall	F1 Measure
Before QSMOTE				
LR	0.9707 \pm 0.0090	0.9718 \pm 0.0099	0.9707 \pm 0.0090	0.9702 \pm 0.0091
RF	0.9752 \pm 0.0166	0.9771 \pm 0.0157	0.9752 \pm 0.0166	0.9748 \pm 0.0169
SVM	0.9775 \pm 0.0071	0.9790 \pm 0.0069	0.9775 \pm 0.0071	0.9771 \pm 0.0071
NB	0.9662 \pm 0.0144	0.9677 \pm 0.0153	0.9662 \pm 0.0144	0.9655 \pm 0.0145
DT	0.9370 \pm 0.0088	0.9428 \pm 0.0109	0.9370 \pm 0.0088	0.9358 \pm 0.0063
After QSMOTE				
LR	0.9882 \pm 0.0068	0.9884 \pm 0.0067	0.9882 \pm 0.0068	0.9882 \pm 0.0068
RF	0.9909 \pm 0.0050	0.9911 \pm 0.0050	0.9909 \pm 0.0050	0.9909 \pm 0.0050
SVM	0.9855 \pm 0.0060	0.9858 \pm 0.0059	0.9855 \pm 0.0060	0.9855 \pm 0.0060
NB	0.9339 \pm 0.0142	0.9378 \pm 0.0149	0.9339 \pm 0.0142	0.9325 \pm 0.0152
DT	0.9783 \pm 0.0101	0.9791 \pm 0.0098	0.9783 \pm 0.0101	0.9780 \pm 0.0104

The results in Table A9 show that QSMOTE considerably improves classifier performance for the hexa-class dataset, with the exception of NB. LR exhibits accuracy gains from 0.9707 ± 0.0090 to 0.9882 ± 0.0068 , along with improvements in precision (0.9718 ± 0.0099 to 0.9884 ± 0.0067), recall (0.9707 ± 0.0090 to 0.9882 ± 0.0068), and F1-score (0.9702 ± 0.0091 to 0.9882 ± 0.0068). RF achieves the highest overall performance, with accuracy increasing from 0.9752 ± 0.0166 to 0.9909 ± 0.0050 , and all other metrics converging above 0.990. SVM also demonstrates notable improvement, as accuracy rises from 0.9775 ± 0.0071 to 0.9855 ± 0.0060 , and F1-score from 0.9771 ± 0.0071 to 0.9855 ± 0.0060 . DT benefits substantially, with accuracy increasing from 0.9370 ± 0.0088 to 0.9783 ± 0.0101 , and F1-score from 0.9358 ± 0.0063 to

0.9780 ± 0.0104 . In contrast, NB experiences a significant drop, with accuracy declining from 0.9662 ± 0.0144 to 0.9339 ± 0.0142 , and F1-score decreasing from 0.9655 ± 0.0145 to 0.9325 ± 0.0152 . Overall, QSMOTE yields strong improvements for LR, RF, SVM, and DT, with RF achieving near-perfect classification results, while NB appears oversensitive to the synthetic data.

Table A10: Performance Metrics of Classical Algorithms Before and After QSMOTE for Hepta-Class Classification on CWRUBD

Algorithm	Accuracy	Precision	Recall	F1 Measure
Before QSMOTE				
LR	0.9701 ± 0.0062	0.9717 ± 0.0057	0.9701 ± 0.0062	0.9688 ± 0.0070
RF	0.9782 ± 0.0170	0.9793 ± 0.0168	0.9782 ± 0.0170	0.9777 ± 0.0177
SVM	0.9661 ± 0.0173	0.9671 ± 0.0178	0.9661 ± 0.0173	0.9654 ± 0.0175
NB	0.9661 ± 0.0101	0.9683 ± 0.0103	0.9661 ± 0.0101	0.9655 ± 0.0106
DT	0.9562 ± 0.0203	0.9588 ± 0.0226	0.9562 ± 0.0203	0.9555 ± 0.0220
After QSMOTE				
LR	0.9767 ± 0.0073	0.9771 ± 0.0071	0.9767 ± 0.0073	0.9766 ± 0.0075
RF	0.9984 ± 0.0019	0.9985 ± 0.0018	0.9984 ± 0.0019	0.9984 ± 0.0019
SVM	0.9860 ± 0.0031	0.9865 ± 0.0032	0.9860 ± 0.0031	0.9860 ± 0.0031
NB	0.9293 ± 0.0045	0.9322 ± 0.0052	0.9293 ± 0.0045	0.9282 ± 0.0050
DT	0.9876 ± 0.0062	0.9881 ± 0.0060	0.9876 ± 0.0062	0.9875 ± 0.0063

The results in Table A10 demonstrate that QSMOTE consistently enhances classifier performance for the hepta-class dataset, with the exception of NB. For LR, the accuracy improves from 0.9701 ± 0.0062 to 0.9767 ± 0.0073 , accompanied by corresponding increases in precision (0.9717 ± 0.0057 to 0.9771 ± 0.0071), recall (0.9701 ± 0.0062 to 0.9767 ± 0.0073), and F1-score (0.9688 ± 0.0070 to 0.9766 ± 0.0075). RF achieves the highest overall performance, with accuracy rising from 0.9782 ± 0.0170 to 0.9984 ± 0.0019 , while all other metrics converge above 0.998. Similarly, SVM improves from 0.9661 ± 0.0173 to 0.9860 ± 0.0031 in accuracy, and from 0.9654 ± 0.0175 to 0.9860 ± 0.0031 in F1-score. DT also benefits considerably, with accuracy increasing from 0.9562 ± 0.0203 to 0.9876 ± 0.0062 and F1-score from 0.9555 ± 0.0220 to 0.9875 ± 0.0063 . In contrast, NB experiences a significant drop after QSMOTE, with accuracy decreasing from 0.9661 ± 0.0101 to 0.9293 ± 0.0045 and F1-score from 0.9655 ± 0.0106 to 0.9282 ± 0.0050 , indicating sensitivity to synthetic sample generation. Overall, QSMOTE boosts the performance of LR, RF, SVM, and DT, with RF achieving near-perfect classification results.

The results in Table A11 show that QSMOTE substantially improves performance across most classifiers for the octa-class dataset. For LR, the accuracy increases from 0.8745 ± 0.0163 to 0.9409 ± 0.0153 , with corresponding gains in precision (0.8945 ± 0.0166 to 0.9448 ± 0.0142), recall (0.8745 ± 0.0163 to 0.9409 ± 0.0153), and F1-score (0.8665 ± 0.0159 to 0.9415 ± 0.0149). RF achieves the strongest results, with accuracy improving from 0.9495 ± 0.0140 to 0.9844 ± 0.0046 , while all other metrics remain above 0.984. Similarly, SVM improves from 0.8780 ± 0.0269 to 0.9341 ± 0.0090 in accuracy,

Table A11: Performance Metrics of Classical Algorithms Before and After QSMOTE for Octa-Class Classification on CWRUBD

Algorithm	Accuracy	Precision	Recall	F1 Measure
Before QSMOTE				
LR	0.8745 \pm 0.0163	0.8945 \pm 0.0166	0.8745 \pm 0.0163	0.8665 \pm 0.0159
RF	0.9495 \pm 0.0140	0.9519 \pm 0.0135	0.9495 \pm 0.0140	0.9487 \pm 0.0148
SVM	0.8780 \pm 0.0269	0.8865 \pm 0.0385	0.8780 \pm 0.0269	0.8613 \pm 0.0255
NB	0.9163 \pm 0.0311	0.9220 \pm 0.0291	0.9163 \pm 0.0311	0.9147 \pm 0.0320
DT	0.9129 \pm 0.0207	0.9239 \pm 0.0134	0.9129 \pm 0.0207	0.9148 \pm 0.0181
After QSMOTE				
LR	0.9409 \pm 0.0153	0.9448 \pm 0.0142	0.9409 \pm 0.0153	0.9415 \pm 0.0149
RF	0.9844 \pm 0.0046	0.9850 \pm 0.0047	0.9844 \pm 0.0046	0.9844 \pm 0.0046
SVM	0.9341 \pm 0.0090	0.9437 \pm 0.0041	0.9341 \pm 0.0090	0.9353 \pm 0.0088
NB	0.8818 \pm 0.0140	0.9056 \pm 0.0087	0.8818 \pm 0.0140	0.8827 \pm 0.0148
DT	0.9790 \pm 0.0084	0.9796 \pm 0.0081	0.9790 \pm 0.0084	0.9789 \pm 0.0085

and from 0.8613 ± 0.0255 to 0.9353 ± 0.0088 in F1-score. In contrast, NB shows a decline after QSMOTE, with accuracy dropping from 0.9163 ± 0.0311 to 0.8818 ± 0.0140 and F1-score decreasing from 0.9147 ± 0.0320 to 0.8827 ± 0.0148 , suggesting oversensitivity to synthetic samples. DT demonstrates notable improvement, with accuracy rising from 0.9129 ± 0.0207 to 0.9790 ± 0.0084 , and F1-score increasing from 0.9148 ± 0.0181 to 0.9789 ± 0.0085 . Overall, QSMOTE enhances minority class representation and leads to strong gains in LR, RF, SVM, and DT, with RF and DT achieving near-optimal classification performance.

Table A12: Performance Metrics of Classical Algorithms Before and After QSMOTE for Nona-Class Classification on CWRUBD

Algorithm	Accuracy	Precision	Recall	F1 Measure
Before QSMOTE				
LR	0.9118 \pm 0.0153	0.9231 \pm 0.0135	0.9118 \pm 0.0153	0.9026 \pm 0.0182
RF	0.9638 \pm 0.0107	0.9669 \pm 0.0099	0.9638 \pm 0.0107	0.9636 \pm 0.0107
SVM	0.9102 \pm 0.0080	0.8963 \pm 0.0324	0.9102 \pm 0.0080	0.8905 \pm 0.0103
NB	0.9638 \pm 0.0080	0.9669 \pm 0.0081	0.9638 \pm 0.0080	0.9635 \pm 0.0080
DT	0.9276 \pm 0.0195	0.9376 \pm 0.0159	0.9276 \pm 0.0195	0.9284 \pm 0.0198
After QSMOTE				
LR	0.9571 \pm 0.0049	0.9582 \pm 0.0041	0.9571 \pm 0.0049	0.9567 \pm 0.0049
RF	0.9934 \pm 0.0044	0.9936 \pm 0.0043	0.9934 \pm 0.0044	0.9933 \pm 0.0045
SVM	0.9656 \pm 0.0123	0.9675 \pm 0.0120	0.9656 \pm 0.0123	0.9653 \pm 0.0126
NB	0.9293 \pm 0.0078	0.9312 \pm 0.0093	0.9293 \pm 0.0078	0.9281 \pm 0.0085
DT	0.9885 \pm 0.0029	0.9890 \pm 0.0028	0.9885 \pm 0.0029	0.9885 \pm 0.0030

The results in Table A12 show a clear improvement in performance metrics after applying QSMOTE to the nona-class dataset. For LR, the accuracy rises from 0.9118 ± 0.0153 to 0.9571 ± 0.0049 , with corresponding gains in precision (0.9231 ± 0.0135 to 0.9582 ± 0.0041), recall (0.9118 ± 0.0153 to 0.9571 ± 0.0049), and F1-score (0.9026 ± 0.0182 to 0.9567 ± 0.0049). RF shows the strongest performance, with accuracy improving from 0.9638 ± 0.0107 to 0.9934 ± 0.0044 , and precision, recall, and F1-score all staying above 0.993. Similarly, SVM improves in accuracy from 0.9102 ± 0.0080 to 0.9656 ± 0.0123 , and in F1-score from 0.8905 ± 0.0103 to 0.9653 ± 0.0126 . On the other hand, NB, while initially competitive with accuracy 0.9638 ± 0.0080 , drops to 0.9293 ± 0.0078 after QSMOTE, along with a slight decrease in F1-score from 0.9635 ± 0.0080 to 0.9281 ± 0.0085 , indicating possible oversampling sensitivity. DT benefits significantly, as accuracy rises from 0.9276 ± 0.0195 to 0.9885 ± 0.0029 , and F1-score increases from 0.9284 ± 0.0198 to 0.9885 ± 0.0030 . Overall, QSMOTE improves the balance of class distributions, leading to performance boosts across most classifiers, with RF and DT showing near-perfect classification performance.

Table A13: Performance Metrics of Classical Algorithms Before and After QSMOTE for Binary-Class Classification on EFDD

Algorithm	Accuracy	Precision	Recall	F1 Measure
Before QSMOTE				
LR	0.7132 ± 0.0146	0.5465 ± 0.0586	0.7132 ± 0.0146	0.6054 ± 0.0149
RF	0.7098 ± 0.0393	0.6518 ± 0.1384	0.7098 ± 0.0393	0.6293 ± 0.0410
SVM	0.7203 ± 0.0019	0.5188 ± 0.0028	0.7203 ± 0.0019	0.6031 ± 0.0026
NB	0.7097 ± 0.0149	0.5458 ± 0.0590	0.7097 ± 0.0149	0.6037 ± 0.0157
DT	0.5910 ± 0.0490	0.6088 ± 0.0324	0.5910 ± 0.0490	0.5978 ± 0.0407
After QSMOTE				
LR	0.5464 ± 0.0653	0.5470 ± 0.0660	0.5464 ± 0.0653	0.5455 ± 0.0657
RF	0.8544 ± 0.0148	0.8618 ± 0.0198	0.8544 ± 0.0148	0.8538 ± 0.0145
SVM	0.7283 ± 0.0380	0.7361 ± 0.0365	0.7283 ± 0.0380	0.7260 ± 0.0391
NB	0.5825 ± 0.0519	0.5837 ± 0.0525	0.5825 ± 0.0519	0.5800 ± 0.0535
DT	0.8132 ± 0.0188	0.8278 ± 0.0306	0.8132 ± 0.0188	0.8114 ± 0.0177

The performance of the classical algorithms for binary-class classification on the Engine Failure Detection Dataset (EFDD) is summarized in Table A13. Prior to applying QSMOTE, SVM achieves the highest accuracy (0.7203 ± 0.0019), while RF exhibits strong precision (0.6518 ± 0.1384) but with considerable variance, reflecting instability under class imbalance. LR and NB produce comparable outcomes, with F1-scores around 0.60, whereas DT lags behind with lower accuracy (0.5910 ± 0.0490). After resampling with QSMOTE, substantial improvements are observed for RF and DT, with RF achieving the best overall performance (accuracy: 0.8544 ± 0.0148 , F1: 0.8538 ± 0.0145) and DT following closely (accuracy: 0.8132 ± 0.0188 , F1: 0.8114 ± 0.0177). SVM also benefits moderately from QSMOTE, with improvements across all metrics, whereas LR and NB show a decline in performance, suggesting oversensitivity.

to the resampled data distribution. These results highlight that ensemble- and tree-based models are more effective and robust for binary classification under imbalanced conditions when augmented with QSMOTE.

Table A14: Performance Metrics of Classical Algorithms Before and After QSMOTE for Tertiary-Class Classification on EFDD

Algorithm	Accuracy	Precision	Recall	F1 Measure
Before QSMOTE				
LR	0.6227 ± 0.0133	0.3983 ± 0.0047	0.6227 ± 0.0133	0.4858 ± 0.0071
RF	0.6073 ± 0.0175	0.4607 ± 0.0618	0.6073 ± 0.0175	0.4955 ± 0.0236
SVM	0.6288 ± 0.0071	0.3986 ± 0.0035	0.6288 ± 0.0071	0.4879 ± 0.0045
NB	0.6196 ± 0.0060	0.4215 ± 0.0511	0.6196 ± 0.0060	0.4884 ± 0.0124
DT	0.4633 ± 0.0519	0.4785 ± 0.0545	0.4633 ± 0.0519	0.4681 ± 0.0502
After QSMOTE				
LR	0.3883 ± 0.0428	0.3866 ± 0.0428	0.3883 ± 0.0428	0.3811 ± 0.0390
RF	0.8769 ± 0.0281	0.8777 ± 0.0282	0.8769 ± 0.0281	0.8756 ± 0.0285
SVM	0.6327 ± 0.0239	0.6321 ± 0.0246	0.6327 ± 0.0239	0.6288 ± 0.0232
NB	0.4177 ± 0.0667	0.4197 ± 0.0714	0.4177 ± 0.0667	0.4163 ± 0.0687
DT	0.8236 ± 0.0421	0.8296 ± 0.0492	0.8236 ± 0.0421	0.8158 ± 0.0432

The results in Table A14 present the performance of five classical machine learning algorithms before and after applying QSMOTE on the third dataset for tertiary-class classification. Before QSMOTE, all models exhibit moderate performance, with SVM achieving the highest accuracy (0.6288 ± 0.0071) and NB achieving the best balance between precision and recall. However, the overall F1-scores remain relatively low, indicating difficulty in handling class imbalance. After applying QSMOTE, significant improvements are observed, particularly for RF and DT, which achieve accuracies of 0.8769 ± 0.0281 and 0.8236 ± 0.0421 , respectively, along with consistently high precision, recall, and F1-scores. In contrast, LR and NB experience performance degradation after resampling, highlighting their sensitivity to oversampled data. The SVM shows stable performance across both settings, with only a slight improvement after QSMOTE. Overall, the findings confirm that ensemble-based methods such as RF and tree-based models like DT are more robust in handling imbalanced datasets when combined with QSMOTE, making them the most effective choices for this classification task.

Table A15 shows the comparative evaluation of classical classifiers before and after QSMOTE for binary classification on Industrial Fault Detection Dataset (IFDD). Before applying QSMOTE, RF (0.8475 ± 0.0080) achieves the best accuracy, followed closely by SVM (0.8454 ± 0.0047) and LR (0.8432 ± 0.0073). Both DT and NB trail with accuracies around 0.70. After QSMOTE, the ensemble and tree-based models exhibit remarkable improvement. RF achieves an almost perfect performance with 0.9900 ± 0.0031 accuracy, marking an absolute gain of +14.3% points. DT follows with 0.8885 ± 0.0172 , a +18.3-point improvement. The SVM classifier also improves modestly to 0.8559 ± 0.0251 , up by +1.05 points. In contrast, LR and NB show slight

Table A15: Performance Metrics of Classical Algorithms Before and After QSMOTE for Binary Classification on IFDD

Algorithm	Accuracy	Precision	Recall	F1 Measure
Before QSMOTE				
LR	0.8432 ± 0.0073	0.7144 ± 0.0082	0.8432 ± 0.0073	0.7735 ± 0.0076
RF	0.8475 ± 0.0080	0.7460 ± 0.0678	0.8475 ± 0.0080	0.7794 ± 0.0148
SVM	0.8454 ± 0.0047	0.7146 ± 0.0080	0.8454 ± 0.0047	0.7745 ± 0.0066
NB	0.7165 ± 0.1439	0.7104 ± 0.0074	0.7165 ± 0.1439	0.6989 ± 0.0952
DT	0.7055 ± 0.0323	0.7222 ± 0.0307	0.7055 ± 0.0323	0.7134 ± 0.0299
After QSMOTE				
LR	0.6241 ± 0.0382	0.6245 ± 0.0380	0.6241 ± 0.0382	0.6237 ± 0.0384
RF	0.9900 ± 0.0031	0.9901 ± 0.0030	0.9900 ± 0.0031	0.9900 ± 0.0031
SVM	0.8559 ± 0.0251	0.8629 ± 0.0253	0.8559 ± 0.0251	0.8552 ± 0.0253
NB	0.6379 ± 0.0448	0.6450 ± 0.0507	0.6379 ± 0.0448	0.6345 ± 0.0436
DT	0.8885 ± 0.0172	0.9083 ± 0.0119	0.8885 ± 0.0172	0.8871 ± 0.0178

declines of -21.9 and -7.9 points, respectively, suggesting that linear and probabilistic models are less adaptive to the synthetic distribution created by QSMOTE. Overall, QSMOTE oversampling significantly benefits non-linear and ensemble classifiers, yielding high precision–recall consistency and near-perfect generalization, particularly in RF and DT, confirming their robustness to class imbalance in binary settings.

Table A16: Performance Metrics of Classical Algorithms Before and After QSMOTE for Tertiary-Class Classification on IFDD

Algorithm	Accuracy	Precision	Recall	F1 Measure
Before QSMOTE				
LR	0.7388 ± 0.0143	0.5614 ± 0.0071	0.7388 ± 0.0143	0.6380 ± 0.0095
RF	0.7425 ± 0.0096	0.5611 ± 0.0067	0.7425 ± 0.0096	0.6392 ± 0.0076
SVM	0.7500 ± 0.0039	0.5625 ± 0.0059	0.7500 ± 0.0039	0.6429 ± 0.0053
NB	0.5571 ± 0.1555	0.5619 ± 0.0159	0.5571 ± 0.1555	0.5342 ± 0.1000
DT	0.5262 ± 0.0269	0.5623 ± 0.0237	0.5262 ± 0.0269	0.5417 ± 0.0185
After QSMOTE				
LR	0.5004 ± 0.0164	0.4920 ± 0.0191	0.5004 ± 0.0164	0.4926 ± 0.0195
RF	0.9925 ± 0.0031	0.9926 ± 0.0030	0.9925 ± 0.0031	0.9925 ± 0.0031
SVM	0.8304 ± 0.0205	0.8313 ± 0.0200	0.8304 ± 0.0205	0.8273 ± 0.0209
NB	0.4929 ± 0.0398	0.4881 ± 0.0455	0.4929 ± 0.0398	0.4799 ± 0.0415
DT	0.8855 ± 0.0057	0.9010 ± 0.0055	0.8855 ± 0.0057	0.8788 ± 0.0064

Table A16 presents the comparative performance of classical classifiers before and after QSMOTE for tri-class classification on the sixth dataset. Before applying QSMOTE, SVM achieves the highest accuracy of 0.7500 ± 0.0039 , followed closely by RF (0.7425 ± 0.0096) and LR (0.7388 ± 0.0143). The NB and DT models show weaker

performance with accuracies of 0.5571 ± 0.1555 and 0.5262 ± 0.0269 , respectively. After applying QSMOTE, the overall performance improves drastically for ensemble and tree-based models. RF attains a near-perfect accuracy of 0.9925 ± 0.0031 , marking a +25.0 % point improvement, while DT reaches 0.8855 ± 0.0057 , improving by +35.9 points. SVM also improves notably to 0.8304 ± 0.0205 , gaining +8.0 points, whereas LR and NB experience minor degradations of approximately -23.8 and -6.4 points, respectively. In terms of precision and F1 measure, RF demonstrate the most consistent and stable performance across all folds (standard deviation ≈ 0.003), signifying strong generalization. The results reaffirm that QSMOTE balancing significantly enhances ensemble and non-linear model performance, whereas linear models like LR and probabilistic ones like NB may not benefit due to overfitting on synthetic minority samples.

References

- [1] Lee, J., Ardakani, H.D., Yang, S., Bagheri, B.: Industrial big data analytics and cyber-physical systems for future maintenance & service innovation. *Procedia CIRP* **38**, 3–7 (2015) <https://doi.org/10.1016/j.procir.2015.08.026>
- [2] Vijayalakshmi, K., Rajakannu, A., Kamaruddin, M., Ramachandran, K.P., Sri Rajkavin, A.V.: Intelligent fault diagnosis of rotating machinery using deep learning algorithms: A comparative analysis of mlp, cnn, rnn, and lstm. *SSRG International Journal of Electrical and Electronics Engineering* **11**(9), 294–315 (2024) <https://doi.org/10.14445/23488379/IJEEE-V11I9P127>
- [3] Chawla, N.V., Bowyer, K.W., Hall, L.O., Kegelmeyer, W.P.: Smote: Synthetic minority over-sampling technique. *Journal of Artificial Intelligence Research* **16**, 321–357 (2002)
- [4] He, H., Garcia, E.A.: Learning from imbalanced data. *IEEE Transactions on Knowledge and Data Engineering* **21**(9), 1263–1284 (2009) <https://doi.org/10.1109/TKDE.2008.239>
- [5] Zhao, J., Wang, W., Huang, J., Ma, X.: A comprehensive review of deep learning-based fault diagnosis approaches for rolling bearings: Advancements and challenges. *AIP Advances* **15**(2), 020702 (2025) <https://doi.org/10.1063/5.0255451>
- [6] Bao, Z., Liu, C., Yang, H., Zhang, J., Li, Y.: From theory to industry: A survey of deep learning-enabled bearing fault diagnosis in complex environments. *Engineering Applications of Artificial Intelligence* **163**(Part 4), 113068 (2026) <https://doi.org/10.1016/j.engappai.2025.113068>
- [7] Preskill, J.: Quantum Computing in the NISQ era and beyond. *Quantum* **2**, 79 (2018) <https://doi.org/10.22331/q-2018-08-06-79>
- [8] Mohanty, N., Behera, B.K., Ferrie, C., Dash, P.: A quantum approach to synthetic

minority oversampling technique (smote). *Quantum Machine Intelligence* **7**(1), 38 (2025) <https://doi.org/10.1007/s42484-025-00248-6>

[9] Schuld, M., Sinayskiy, I., Petruccione, F.: An introduction to quantum machine learning. *Contemporary Physics* **56**(2), 172–185 (2015) <https://doi.org/10.1080/00107514.2014.964942>

[10] Biamonte, J., Wittek, P., Pancotti, N., Rebentrost, P., Wiebe, N., Lloyd, S.: Quantum machine learning. *Nature* **549**(7671), 195–202 (2017) <https://doi.org/10.1038/nature23474>

[11] Dallaire-Demers, P.-L., Killoran, N.: Quantum generative adversarial networks. *Physical Review A* **98**(1), 012324 (2018) <https://doi.org/10.1103/PhysRevA.98.012324>

[12] Kieferová, M., Wiebe, N.: Tomography and generative training with quantum boltzmann machines. *Physical Review A* **96**(6), 062327 (2017) <https://doi.org/10.1103/PhysRevA.96.062327>

[13] Vashishtha, G., Chauhan, S., Sehri, M., Zimroz, R., Dumond, P., Kumar, R., Gupta, M.K.: A roadmap to fault diagnosis of industrial machines via machine learning: A brief review. *Measurement* **242**(Part D), 116216 (2025) <https://doi.org/10.1016/j.measurement.2024.116216>

[14] Blagus, R., Lusa, L.: Smote for high-dimensional class-imbalanced data. *BMC Bioinformatics* **14**(1), 106 (2013) <https://doi.org/10.1186/1471-2105-14-106>

[15] Fernández, A., García, S., Galar, M., Prati, R.C., Krawczyk, B., Herrera, F.: Learning from Imbalanced Data Sets. Springer Series in Statistics. Springer, Cham (2018). <https://doi.org/10.1007/978-3-319-98074-4>

[16] McClean, J.R., Romero, J., Babbush, R., Aspuru-Guzik, A.: The theory of variational hybrid quantum–classical algorithms. *New Journal of Physics* **18**(2), 023023 (2016) <https://doi.org/10.1088/1367-2630/18/2/023023>

[17] Benedetti, M., Lloyd, E., Sack, S., Fiorentini, M.: Parameterized quantum circuits as machine learning models. *Quantum Science and Technology* **4**(4), 043001 (2019) <https://doi.org/10.1088/2058-9565/ab4eb5>

[18] Han, H., Wang, W.-Y., Mao, B.-H.: Borderline-smote: A new over-sampling method in imbalanced data sets learning. *Proceedings of the 2005 International Conference on Advances in Intelligent Computing (ICIC'05)*, Volume Part I, 878–887 (2005) https://doi.org/10.1007/11538059_91

[19] He, H., Bai, Y., Garcia, E.A., Li, S.: Adasyn: Adaptive synthetic sampling approach for imbalanced learning. *IEEE International Joint Conference on Neural Networks*, 1322–1328 (2008) <https://doi.org/10.1109/IJCNN.2008.4633969>

- [20] Batista, G.E., Prati, R.C., Monard, M.C.: A study of the behavior of several methods for balancing machine learning training data. *SIGKDD Explorations* **6**(1), 20–29 (2004) <https://doi.org/10.1145/1007730.100773>
- [21] Bhuiyan, M.R., Uddin, J.: Deep transfer learning models for industrial fault diagnosis using vibration and acoustic sensors data: A review. *Vibration* **6**(1), 218–238 (2023) <https://doi.org/10.3390/vibration6010014>
- [22] Wang, H., Wang, H., Tang, X.: A review of deep learning in rotating machinery fault diagnosis and its prospects for port applications. *Applied Sciences* **15**(21), 11303 (2025) <https://doi.org/10.3390/app152111303>
- [23] Lo, N.G., Flaus, J.-M., Adrot, O.: Review of machine learning approaches in fault diagnosis applied to iot systems. 2019 International Conference on Control, Automation and Diagnosis (ICCAD) (2019) <https://doi.org/10.1109/ICCAD46983.2019.9037949>
- [24] Rish, I.: An Empirical Study of the Naive Bayes Classifier. Technical Report, IBM Research (2001)
- [25] Vapnik, V.N.: An overview of statistical learning theory. *IEEE Transactions on Neural Networks* **10**(5), 988–999 (1999) <https://doi.org/10.1109/72.788640>
- [26] Breiman, L.: Random forests. *Machine Learning* **45**(1), 5–32 (2001) <https://doi.org/10.1023/A:1010933404324>
- [27] Szegedy, C., Zaremba, W., Sutskever, I., *et al.*: Intriguing properties of neural networks. In: arXiv:1312.6199 (2014). <https://doi.org/10.48550/arXiv.1312.6199>
- [28] Hendrycks, D., Dietterich, T.: Benchmarking neural network robustness to common corruptions and perturbations. (2019). <https://doi.org/10.48550/arXiv.1903.12261>
- [29] Song, Q., Sun, S., Wang, B., Song, Q., Wang, T., Jiang, H.: Noise-robust fault diagnosis network based on multiscale feature enhancement and dynamic cross-modal interaction. *Measurement* **257**(Part A), 118564 (2026) <https://doi.org/10.1016/j.measurement.2025.118564>
- [30] Nielsen, M.A., Chuang, I.L.: Quantum computation and quantum information (2002) <https://doi.org/10.1017/CBO9780511976667>
- [31] Schuld, M., Killoran, N.: Quantum machine learning in feature hilbert spaces. *Physical Review Letters* **122**(4), 040504 (2019) <https://doi.org/10.1103/PhysRevLett.122.040504>
- [32] Khanal, B., Rivas, P.: Learning robust observable to address noise in quantum machine learning. arXiv preprint arXiv:2409.07632 (2024) <https://doi.org/>

10.48550/arXiv.2409.07632 arXiv:2409.07632 [quant-ph]

[33] Afroz, P.: Solar Panel Images Dataset. <https://www.kaggle.com/datasets/pythonafroz/solar-panel-images>. Kaggle Dataset. Accessed: 2025-09-01

[34] brjapon: CWRU Bearing Datasets. <https://www.kaggle.com/datasets/brjapon/cwru-bearing-datasets>. Kaggle dataset. Accessed: 2025-09-26

[35] ziya07: Engine Failure Detection Dataset. <https://www.kaggle.com/datasets/ziya07/engine-failure-detection-dataset>. Kaggle dataset. Accessed: 2025-09-30

[36] Programmer3: Industrial Fault Detection Dataset. <https://www.kaggle.com/datasets/programmer3/industrial-fault-detection-dataset>. Kaggle dataset. Accessed: 2025-10-01

[37] Satpathy, S.K., Vibhu, V., Behera, B.K., Al-Kuwari, S., Mumtaz, S., Farouk, A.: Analysis of quantum machine learning algorithms in noisy channels for classification tasks in the iot extreme environment. IEEE Internet of Things Journal **11**(3), 3840–3852 (2023) <https://doi.org/10.1109/JIOT.2023.3300577>